Siemens Healthineers Headquarters
Siemens Healthcare GmbH
Henkestr. 127
91052 Erlangen
Germany
Phone: +49 9131 84-0
siemens.com/healthineers

Published by Siemens Healthcare GmbH · Order No. A91MR-1100-97C-7600 · Printed in Germany · 6252 06180.1w5 · ©Siemens Healthcare GmbH, 2018

High-end Performance in Musculoskeletal Imaging

MAGNETOM Vida Clinical Case Studies

Axel Stäbler, M.D.
Radiologie in München Harlaching, Munich, Germany

GOKnee3D – Fully-automated One-button-push High-resolution MRI of the Knee

Jan Fritz, M.D., P.D., D.A.B.R.; Filippo Del Grande, M.D., MBA, MHEM; Neil Kumar, M.D.; Derek F Papp, M.D.; Rushyuan J Lee, M.D.
Johns Hopkins University School of Medicine, Baltimore, MD, USA

Metal Artifact Reduction Sequence (MARS) Magnetic Resonance Neurography (MRN) Evaluation of the Lumbosacral Plexus in Patients with Metallic Implants

Shivani Ahlawat, M.D.; Jan Fritz, M.D., P.D., D.A.B.R.
Johns Hopkins University School of Medicine, Baltimore, MD, USA

Reprinted from MAGNETOM Flash (69) 3/2017

SIEMENS Healthineers

MAGNETOM Vida Clinical Case Studies

Axel Stäbler, M.D.

Radiologie in München Harlaching, Munich, Germany

Case 1

8-year-old boy with Legg-Calvé-Perthes disease left hip. Coronal PDw fatsat and T1w, axial and sagittal PDw fatsat. Legg-Calvé-Perthes disease causes aseptic necrosis of the femoral head in children, mainly between the ages of five and eight. The whole of the left femoral head epiphysis is fragmented and severely flattened, there is a reduction of more than 50% in the height of the lateral pillar, and the epiphysis has been displaced laterally from the hip joint cavity. The acetabulum, too, is already deformed and flattened; signal intensity for the acetabular labrum is regular, low. Only remnants of the epiphyseal nucleus are still visible; the growth plate and adjacent metaphysis are involved, widened, and deformed. Coxa magna.

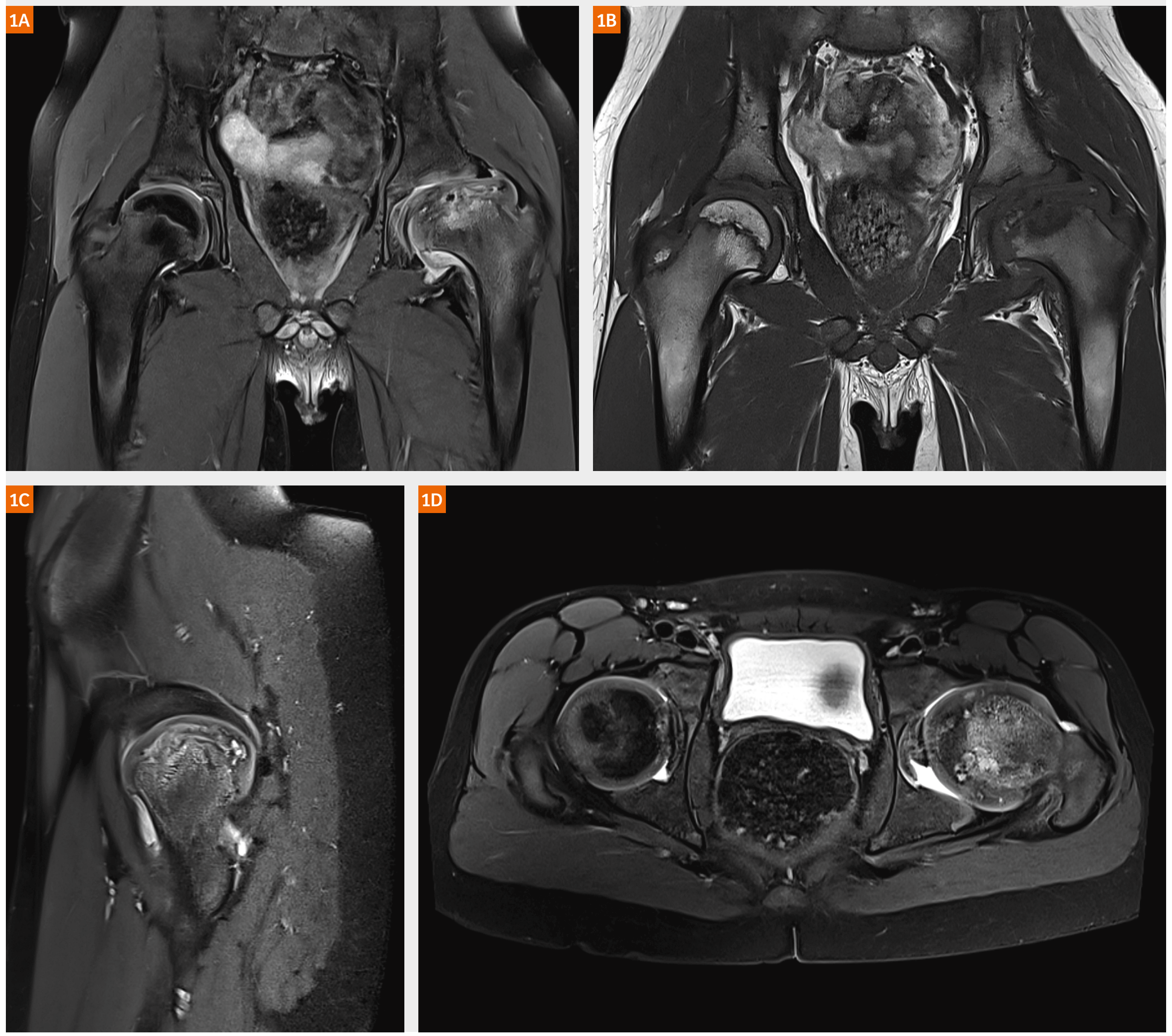

Case 2

73-year-old patient with activated coxarthrosis, right. Coronal PDw fatsat and T1w, sagittal PDw fatsat of the right and left hip. The joint space in the right hip joint is completely narrowed; there is a large resorption cyst in the cranial pressure absorption zone, with active edemata in the femoral neck up to the intertrochanteric region. The left hip, which is still largely normal, is shown for comparison.

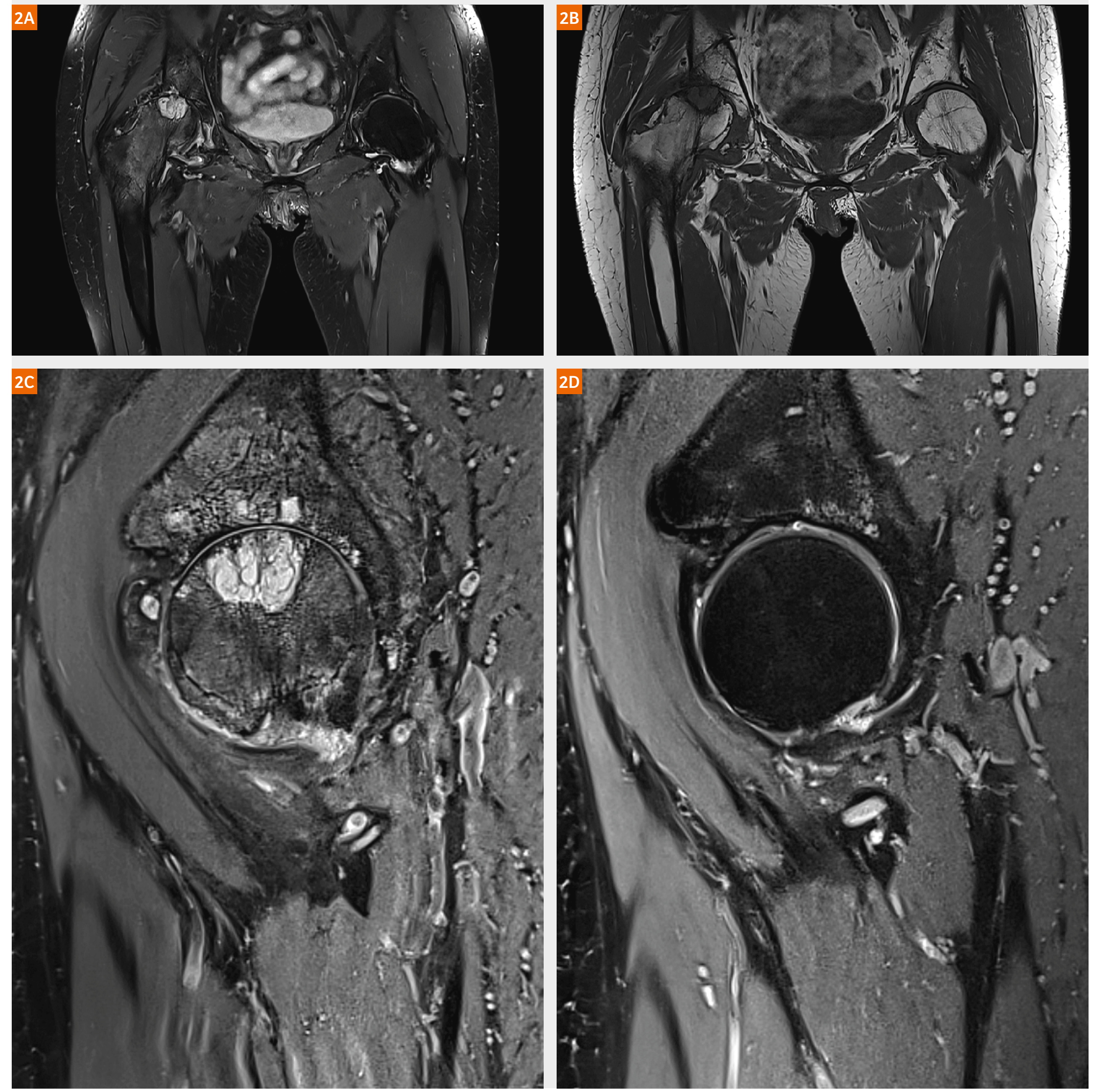

Case 3

61-year-old male with plantar plate rupture at DII. The sagittal PDw fatsat image shows a tear in the plantar plate. There has been fraying/disintegration of the fibrous sheath around the flexor tendon, so the flexor tendon can be differentiated from the plantar plate. The plantar plate is proximally dislocated and extends beyond the condyle in the direction of the metaphysis. The base of the proximal phalanx is slightly decentered towards the dorsum of the foot. MTP joint III is pictured for comparison to show the normal alignment. In the axial T1w image, the flexor tendon is laterally subluxated; with its split/broken down fibrous sheath, it can be differentiated as an exposed structure. The plantar plate has a medial tear and cannot be differentiated. The T1w fatsat, following administration of contrast medium, shows the same result.

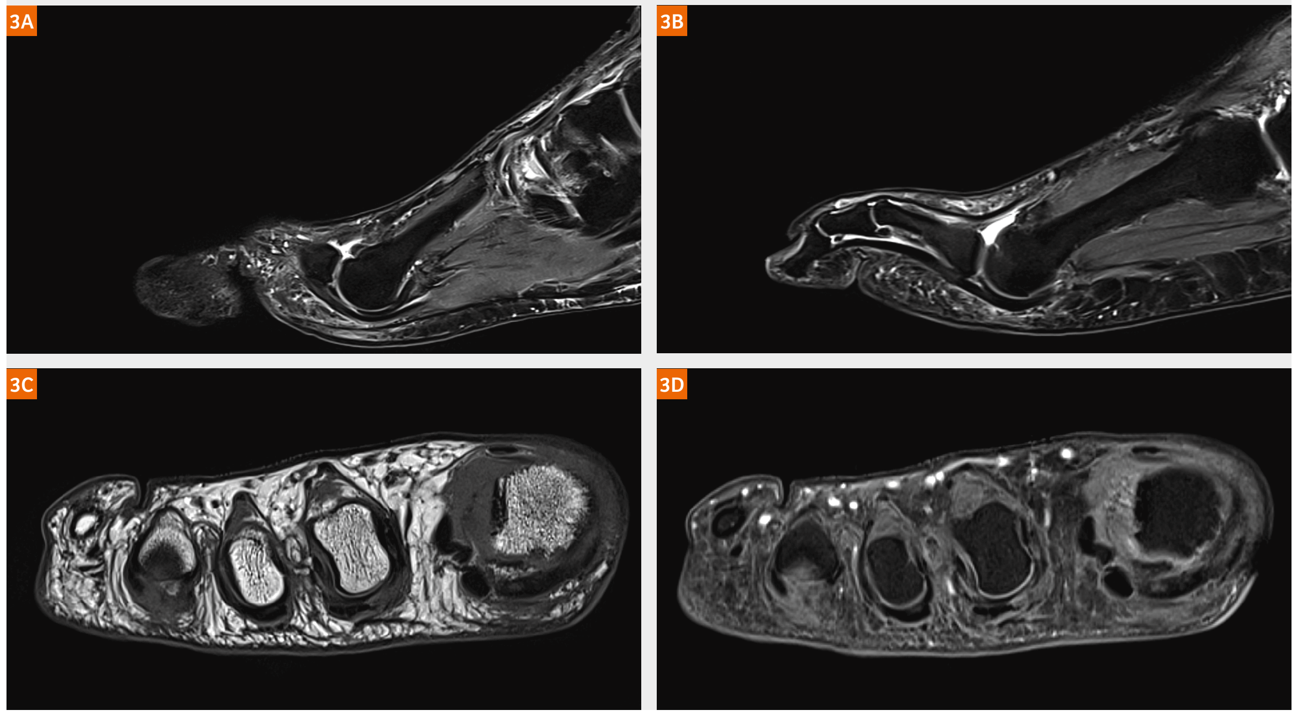

Case 4

38-year-old male, presented with symptoms after fracture of distal fibula eight weeks earlier. The coronal T1w and PDw fatsat images show a persistent Weber type A fracture of distal fibula. The increase in signal intensity in the bone marrow, focused on the subcortical zone, that appear in the PDw fatsat images are indicative of reactive bone marrow change associated with bone dystrophy. There is anterolateral luxation of the peroneal tendons, as well as an anteromedial luxation of the tendon of the tibialis posterior (at the level of the medial malleolus). The axial T2w image shows the medially luxated posterior tibial tendon; at this level, the retinacula of the peroneal tendons are still intact. Anterolateral luxation of the peroneal tendons is shown in the next image. This can also be seen in the oblique axial PDw fatsat image (tendon tilt).

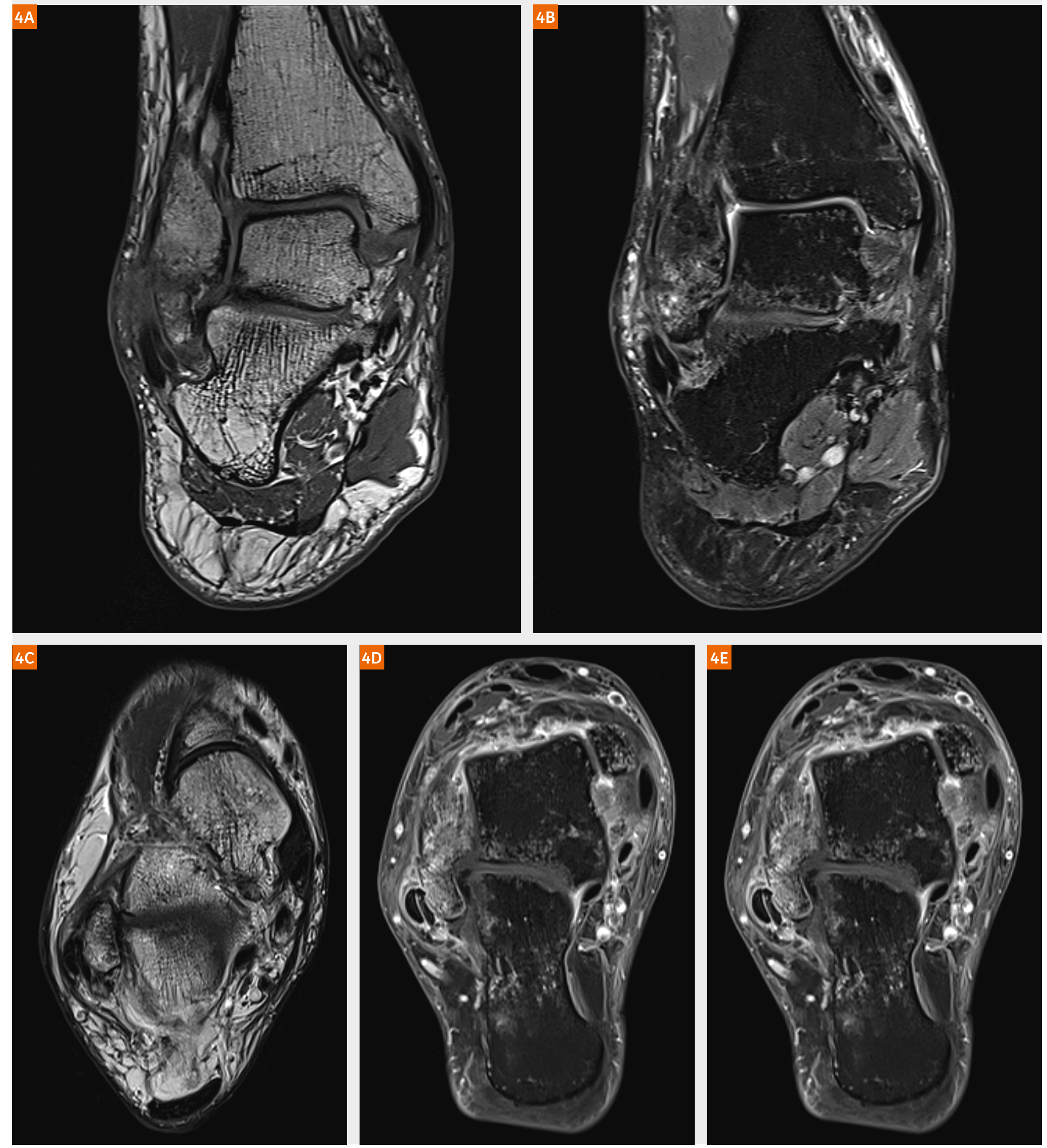

Reprinted from MAGNETOM Flash (69) 3/2017
www.siemens.com/magnetom-world

Case 5

70-year-old male with advanced medial gonarthrosis presenting with femoral and tibial chondropathy (grade IV), degenerative disintegration of the medial meniscus, and osteophytic outgrowths (PDw fatsat and coronal T1w). In the PDw fatsat images, extensive cartilage damage and incipient bone loss on the tibial plateau are visible in the medial compartment. In the sagittal image (PDw fatsat) osteophytic spurs at the upper and lower pole of the patella are clearly visible.

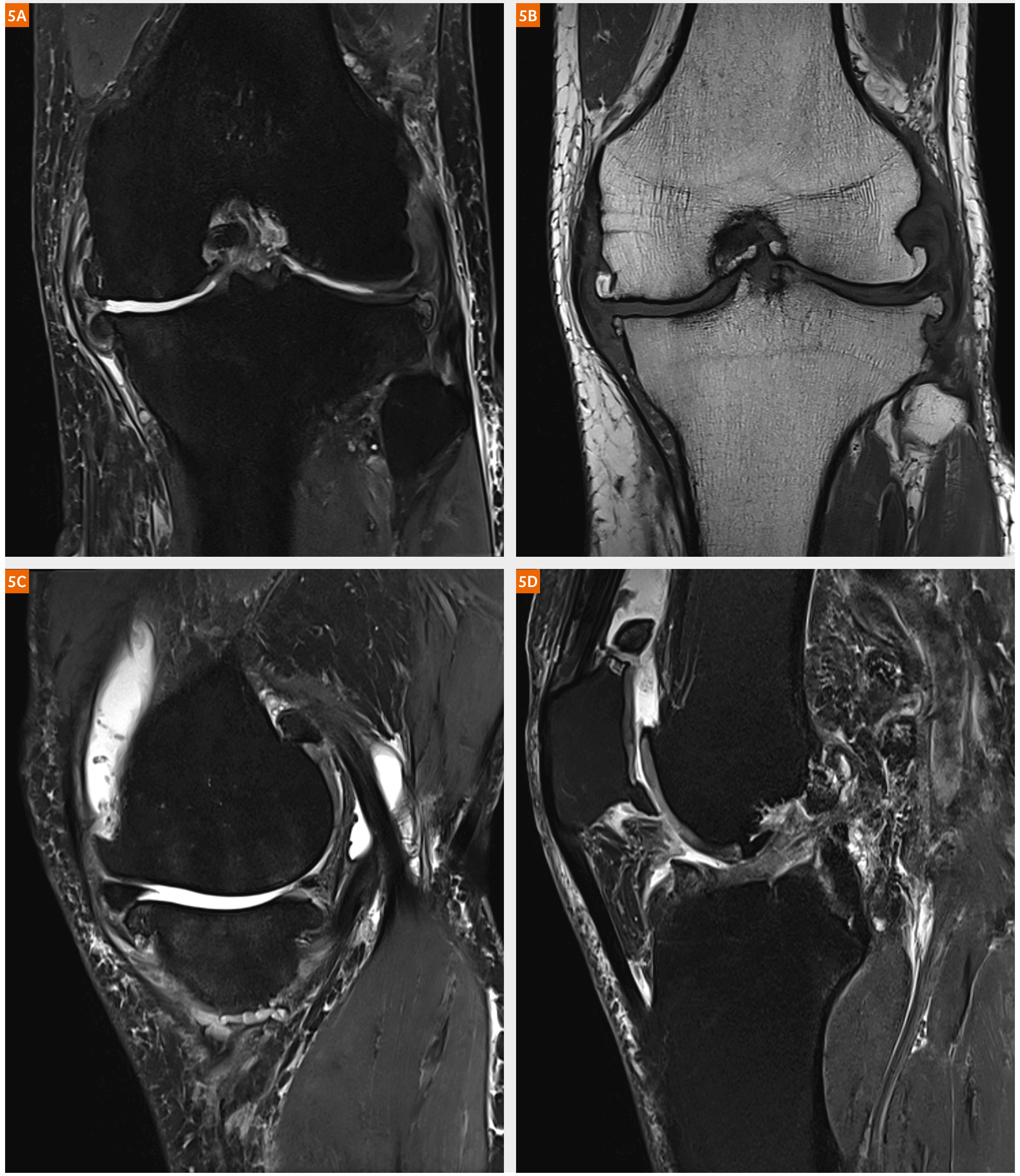

Reprinted from MAGNETOM Flash (69) 3/2017
www.siemens.com/magnetom-world

Case 6

54-year-old male with post-traumatic quadriceps tendon rupture (sagittal PDw fatsat and PDw). The rupture occurred at the osseotendinous junction at the superior pole of the patella, marked surrounding edema and effusion and downward angulation of the patella.

Case 7

57-year-old male with degenerative tearing of the foveal attachments of the discus articularis, leading to instability in the distal radioulnar joint with effusion and fibrovascular scar tissue around the capsule (coronal PDw fatsat, T1w fatsat after intravenous administration of contrast medium, axial T2w).

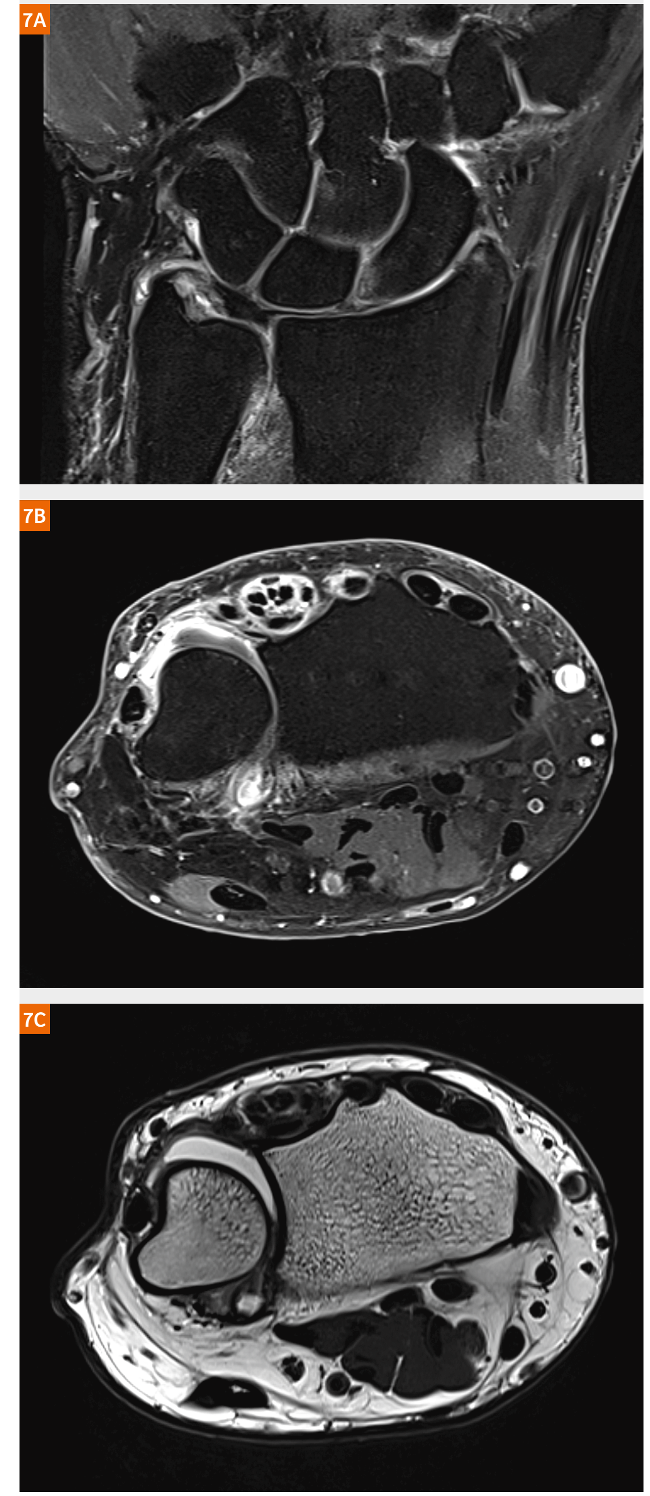

Case 8

86-year-old male with active medial meniscus lesion, an acute meniscal tear of the medial posterior horn. There is vertical-radial tearing with an additional longitudinal rupture, indicative of complex tearing (coronal, axial and sagittal PDw fatsat, coronal T1w).

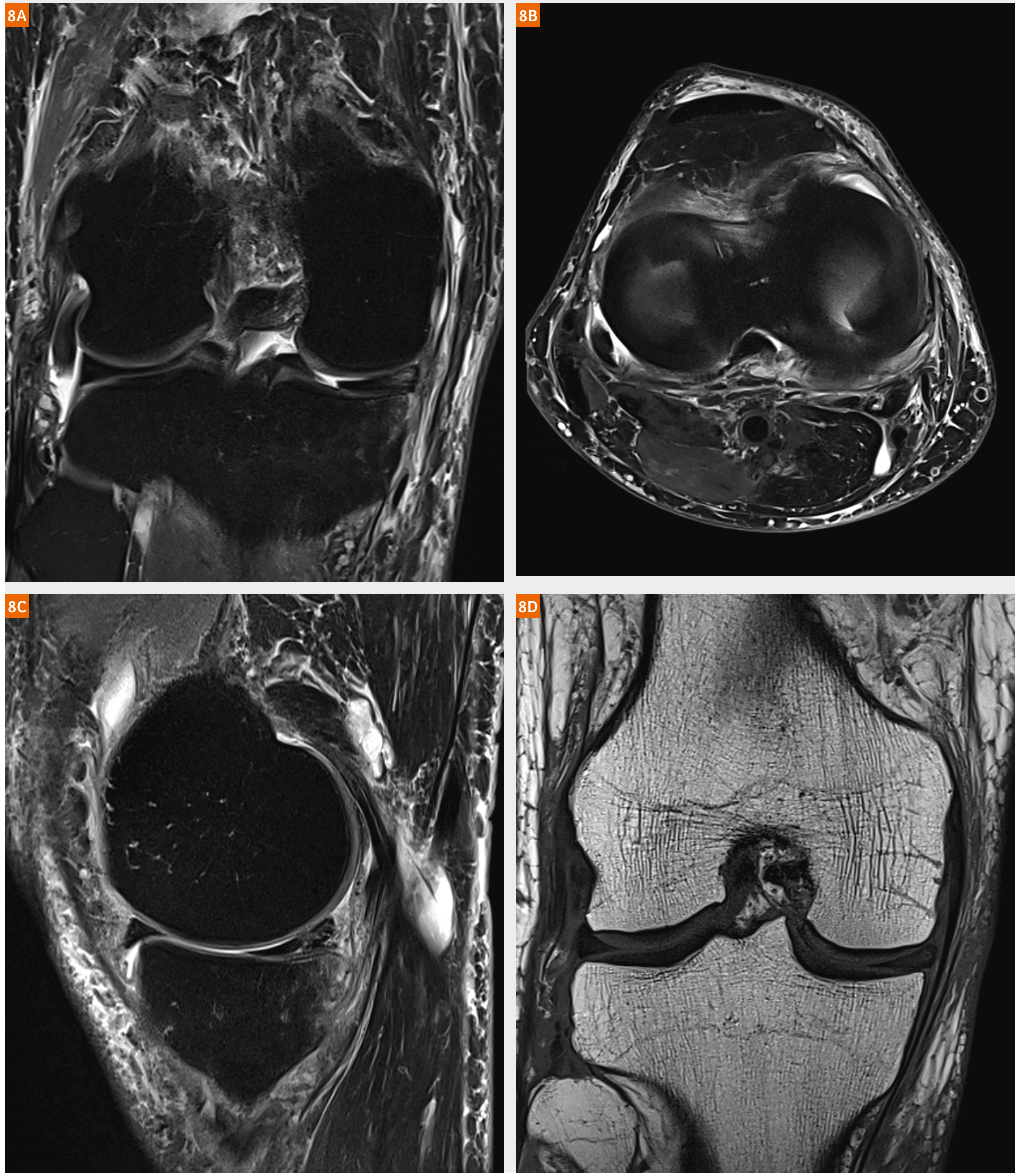

Case 9

53-year-old male with right-sided foraminal disc sequestration at L3/4. The case demonstrates extrusion of disc tissue into the epidural space with cranial migration. The disc tissue is brighter in the T2w image than the original disc during fluid inflow. Signal intensity for the sequestered disc is low in the T1w image and very high in the STIR image. Sequestration was caused by a fibrous ring lesion, visible in the axial T2w image, with displacement of the extraforaminal root L3, right.

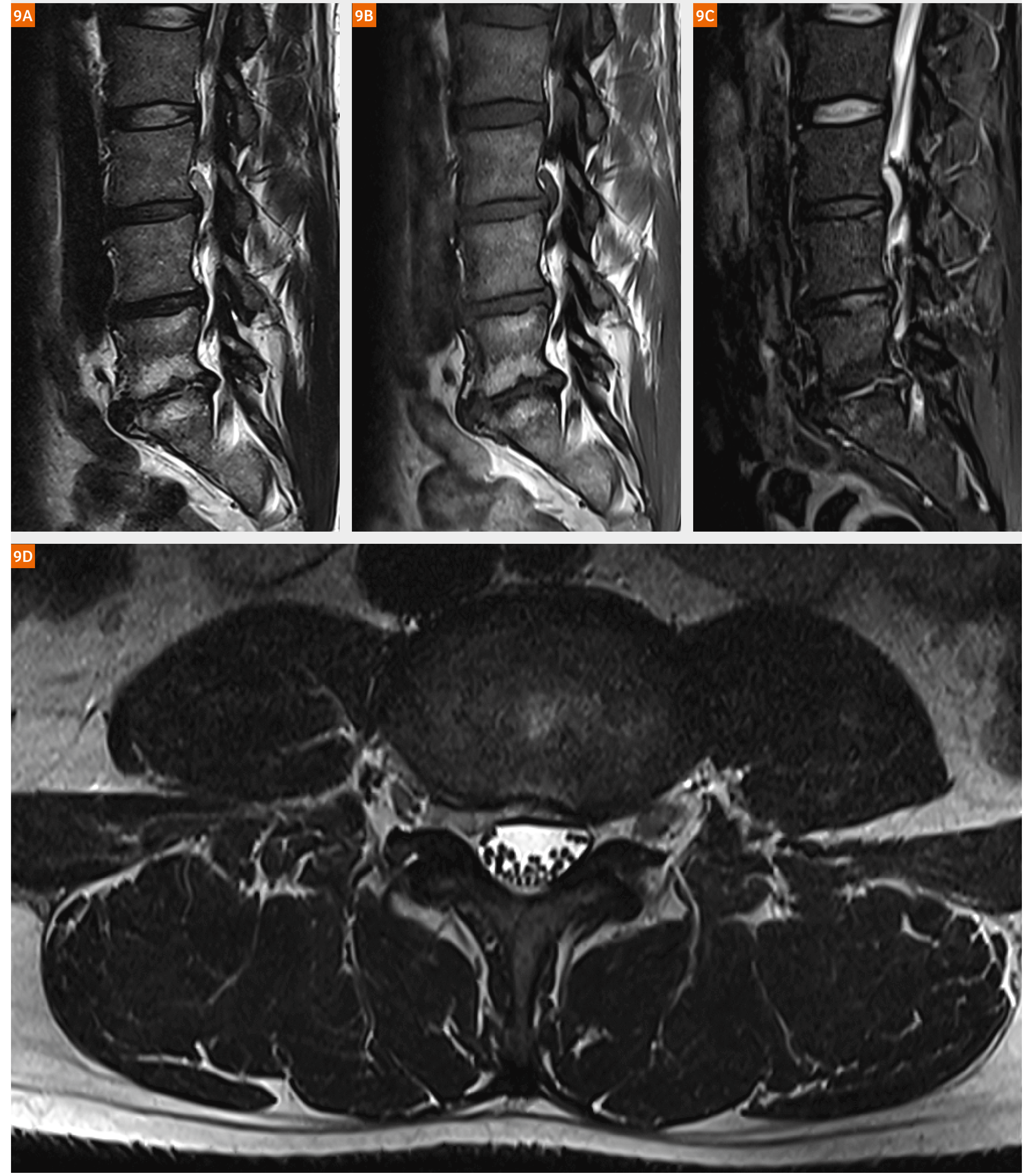

Case 10

32-year-old female with rheumatoid arthritis. The PDw fatsat image shows severe thinning of the supraspinatus tendon, with extensive glenohumeral cartilage damage (grade III–IV). There has been inflammatory bone resorption in the "bare area" and the "footprint" of the supraspinatus tendon. Signal intensity for this is low in the T1w image and is moderately enhanced in the T1w fatsat image after administration of contrast medium. Proliferative synovitis, an effusion, and synovial proliferations (enhanced by contrast medium) are visible on the axial PDw fatsat and T1w fatsat image.

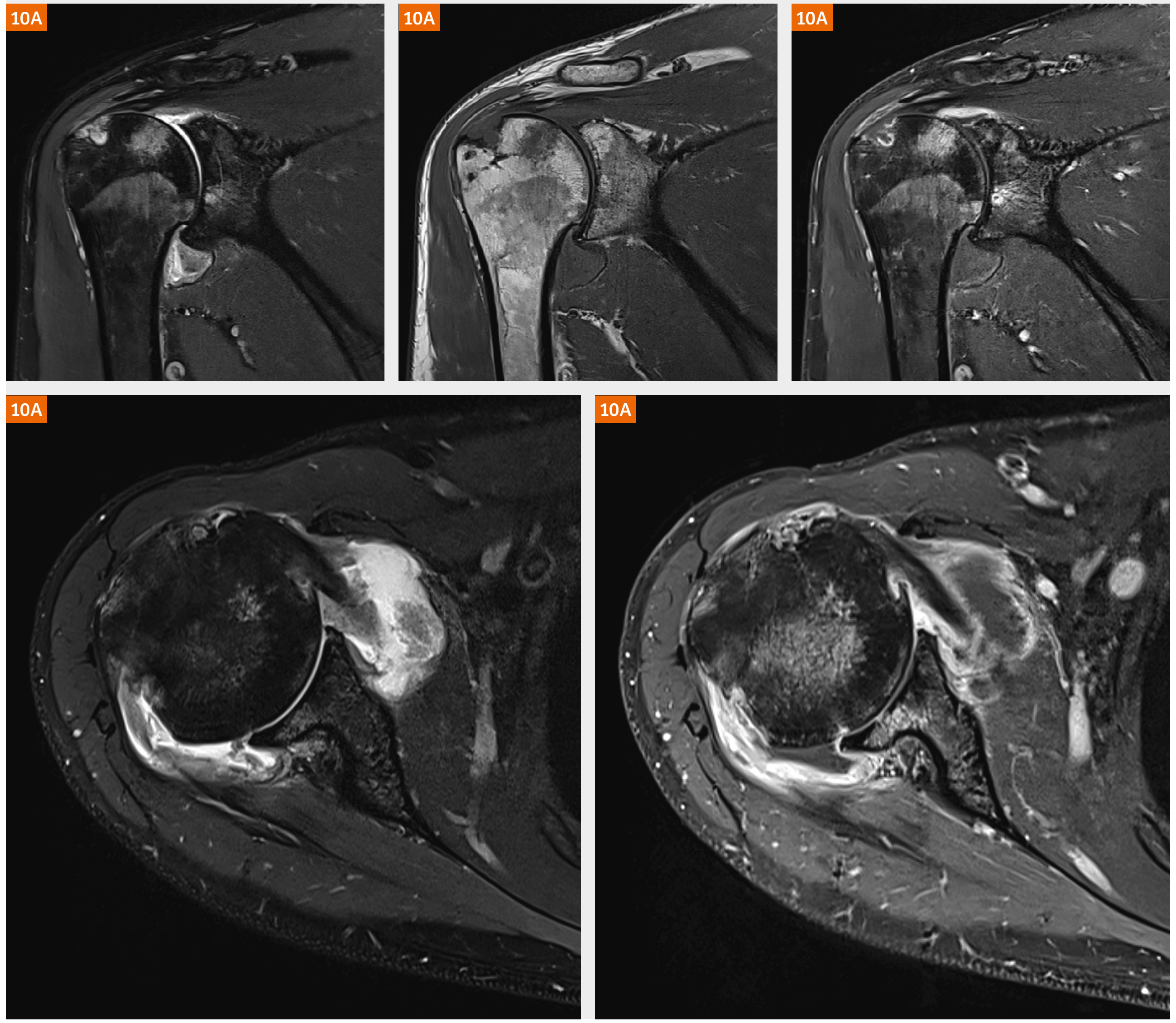

Contact

Professor Axel Stäbler, M.D.
Radiologie in München Harlaching

Grünwalder Straße 72
81547 Munich
Germany
+49 (0)89 6202 1630
staebler@radiologie-muenchen-harlaching.de

GOKnee3D – Fully-automated One-button-push High-resolution MRI of the Knee

Jan Fritz, M.D., P.D., D.A.B.R.; Filippo Del Grande, M.D., MBA, MHEM; Neil Kumar, M.D.; Derek F Papp, M.D.; Rushyuan J Lee, M.D.

Johns Hopkins University School of Medicine, Baltimore, MD, USA

Magnetic resonance imaging (MRI) plays a key role in the workup of acute and chronic injuries, pain syndromes, and dysfunction of the knee. While radiographic and computed tomography evaluations provide excellent osseous detail, MRI is most accurate for the detection of bone marrow edema in the setting of radiographically occult bone contusion injuries and osseous stress reactions, non-displaced fractures, acute chondral shear injuries, and degenerative cartilage defects, tears of the collateral and cruciate ligaments, muscle-tendon injuries, and meniscal tears. Also, MRI can diagnose synovitis not only by the presence of a joint effusion, but also by visualizing synovial thickening, edema pattern, and frond-like hypertrophy.

Most MRI protocols of the knee for the assessment of internal derangement include pulse sequences that are tailored for the morphological assessment of anatomic structures, as well as pulse sequences that are tailored to maximize the conspicuity of findings with long T2 constants, such as fluid and edema.

For morphological assessment of the integrity of anatomical structures, intermediate-weighted MR images with echo times around 30 ms and no fat suppression are ideally suited due to their high signal yield, intermediate-to-high fluid signal, and high contrast-to-noise ratios of low signal intensity structures such as menisci, ligaments, and cartilage. The addition of a T1-weighted pulse sequence to the protocol can be beneficial for bone marrow assessment due to their exquisite specificity for fat signal, including osteomyelitis, marrow replacing diseases, and possibly fractures. However, T1-weighted pulse sequences have a lower sensitivity for detecting cartilage defects, ligamentous injuries, and meniscal tears due to absent fluid signal. Structural pulse sequences are often designed with a higher spatial resolution to maximize structural detail and the detection of small abnormalities, such cartilage fissures, and coapted tears.

For the assessment of signal abnormalities, pulse sequences with longer echo times and fat suppression

1

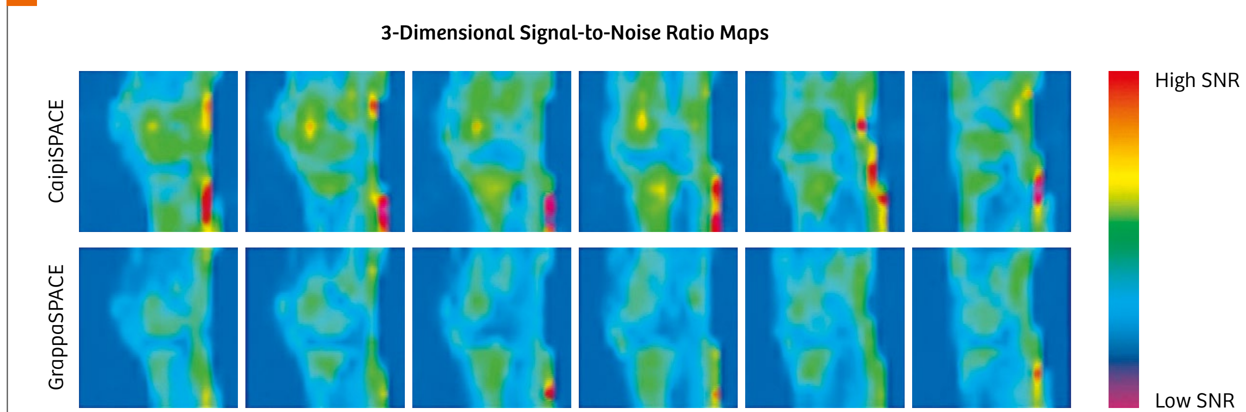

Figure 1:
3-Dimensional Signal-to-Noise Ratio maps illustrate the higher signal yield of CAIPIRINHA-accelerated 3D SPACE over GRAPPA-accelerated 3D SPACE.

510(k) pending. The product is not commercially available. Future availability cannot be guaranteed.

are typically used to increase the conspicuity of findings with long T2 constants, such as joint fluid, collections, and edema. The presence of an edema pattern in bone, ligaments, muscles, and fatty tissues often allows the differentiation of an acute injury or inflammation from chronic remodeling. Abnormally T2 hyperintense areas also have a higher suspicion to be a pain generator. Fast and turbo spin echo (TSE) pulse sequences with effective echo times of 60–70 ms and spectral fat suppression result in exquisite fluid sensitivity. The use of Spectral Attenuated Inversion Recovery (SPAIR) technique, instead of conventional spectral fat suppression can improve the homogeneity of fat suppression across the field-of-view [1]. Alternatively, STIR (Short Tau Inversion Recovery) technique may be used. Fluid sensitive sequences can be designed with less spatial resolution, as it does not interfere with their fluid-sensitivity but can improve efficiency and compensate for the lack of signal from suppressed fat-bound protons.

Two-dimensional (2D) TSE pulse sequences can be acquired with a high in-plane spatial resolution, e.g., with a pixel size of 0.5 x 0.5 mm^2 and less. However, to gain enough MR signal, a slice thickness of 2–4 mm is required, which lowers the effective spatial resolution and results in partial volume effects. The anisotropic voxel size prevents multiplanar reformations and requires the separate acquisition of images in axial, sagittal, and coronal orientation, which can be a time-consuming process and often requires total protocol acquisition times of 20 minutes.

Three dimensional (3D) TSE techniques such as Sampling Perfection with Application optimized Contrast using different flip angle Evolutions (SPACE) yield markedly more MR signal, due to volume-based excitation and use of multiple additional phase-encoding steps in a second direction. Together with the much higher signal yield, 3D data sets allow for the generation of much thinner slices partitions and facilitate 3D MRI with isotropic voxels size.

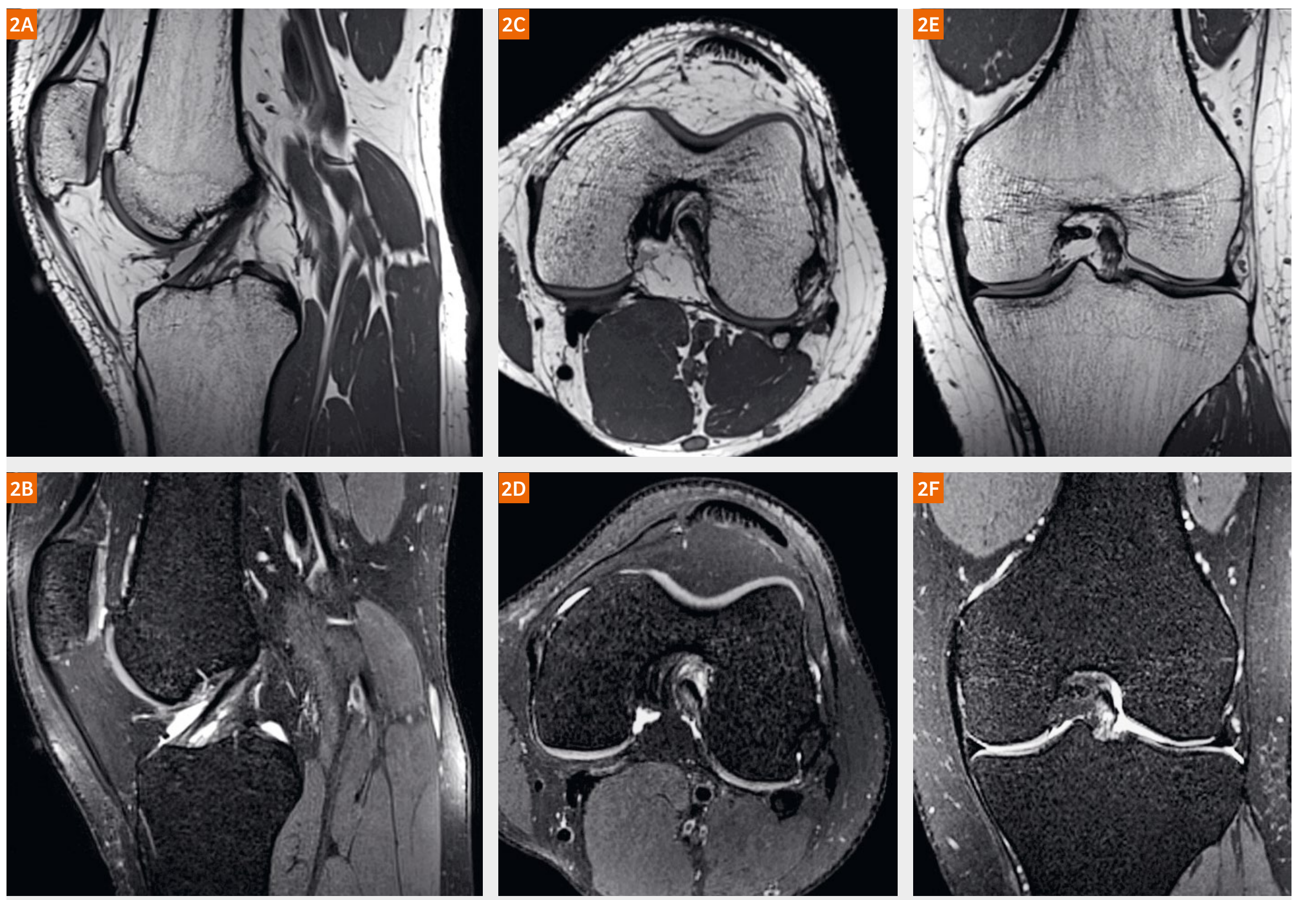

Figure 2:
Normal left knee of a 37-year-old healthy man. Sagittal isotropic 0.5 mm intermediate-weighted and 0.6 mm T2-SPAIR-weighted 3D CAIPIRINHA SPACE source MR images **(2A, B)** with standard axial **(2C, D)** and coronal **(2E, F)** reformats.

3

AA Scout	IW 3D CAIPIRINHA SPACE	TSFS 3D CAIPIRINHA SPACE
13 sec	4 min 41 sec	4 min 45 sec
Total Scan Time: 9 min 39 sec		

Figure 3:
GOKnee3D protocol for 3T MRI of the knee in under 10 minutes.

Such isotropic data sets with sufficiently small voxel size virtually eliminate partial volume effects and provide an opportunity for the improved display of small anatomic detail. Also, virtually any imaging plane can be reformatted from a single parent dataset (Fig. 1), including standard axial, sagittal, and coronal MR images, as well as oblique and curved planar reformations and 3D volume-rendered MR images.

The two phase-encoding directions of 3D SPACE provide an opportunity for bi-directional acceleration. A 2 x 2 parallel imaging using a Generalized Autocalibrating Partial Parallel Acquisition (GRAPPA) sampling pattern facilitates a 4-fold acceleration without the occurrence of acceleration and aliasing artifacts. As a further development, the use of a shifted Controlled Aliasing In Parallel Imaging Results IN Higher Acceleration (CAIPIRINHA) sampling pattern results in the optimized use of differential coil spatial sensitivities and improved geometry (g) factor performance [2, 3]. When compared to GRAPPA SPACE, CAIRPINIHA SPACE is characterized by increased image quality and 10–20% higher signal-to-noise ratios (Fig. 1). CAIPIRINHA-based 4-fold acceleration substantially reduces the time required for data acquisition and eliminates the need for compromises, including long echo trains, partial Fourier undersampling, and anisotropic data acquisition (Fig. 2) [4–6]. CAIPIRINHA SPACE with integrated anatomical landmark-based AutoAlign Knee technology, which provides automatic field-of-view and slice positioning, builds the foundation for GOKnee3D – a fully automated, one-button-push, high-resolution, 3D isotropic diagnostic knee exam with intermediate- and T2-SPAIR-weighted image contrasts and a total acquisition time of fewer than 10 minutes (Fig. 3).

The development of GOKnee3D adopted a similar strategic approach as earlier GO (Generalized Optimized) strategies [7–9]. The clinical validation study of GOKnee3D included head-to-head comparisons with conventional exams of 100 patients that were scanned at the MAGNETOM Skyra (3T) and 50 patients that were scanned at the MAGNETOM Aera (1.5T) [10]. All patients underwent the 10-minute GOKnee3D exam as well as a high-quality conventional 20-minute 2D exam that included six separately acquired pulse sequences of standard non-fat-suppressed and fat-suppressed clinical contrasts in three orientations. All images were independently evaluated by two board-certified, fellowship-trained musculoskeletal radiologists. The images were assessed for the presence or absence of joint effusion, joint bodies, popliteal cysts, lateral and medial meniscal tears, medial and lateral collateral ligament tears, anterior and posterior cruciate ligament tears, quadriceps and patella tendon tears, cartilage defects, bone marrow edema, and fractures. Additionally, the overall image quality and severity of motion artifact were also evaluated.

The study results indicate that the images generated by the 10-minute GOKnee3D protocol are at least diagnostically equivalent to the images of a 20-minute 2D TSE standard of reference protocol. There were no significant differences in the diagnosis of abnormal findings between GOKnee3D and the 2D TSE exams at both 1.5T and 3T. For both, 1.5T and 3T GOKnee3D protocols, the inter-reader agreement was consistently higher for the 3D images when compared to the 2D images.

An ongoing study evaluating the diagnostic accuracy of GOKnee3D for the detection of internal derangement in children[1] and adolescents, with arthroscopy as the standard of reference, indicates sensitivities of 83–100% and specificities of 93–100% for the diagnoses of discoid menisci, meniscus tears, ligament injuries, and osteochondritis dissecans lesions [11]. This study is currently being extended to adult patients.

The following clinical cases with surgical correlation illustrate the application of GOKnee3D for the evaluation of internal derangement in adults and children. All images were acquired on a 3T MAGNETOM Skyra MR imaging system (Siemens Healthcare, Erlangen, Germany) and Tx/Rx Knee 15 (QED, Mayfield Village, OH, USA) surface coil.

[1] MR scanning has not been established as safe for imaging fetuses and infants less than two years of age. The responsible physician must evaluate the benefits of the MR examination compared to those of other imaging procedures.

Case 1

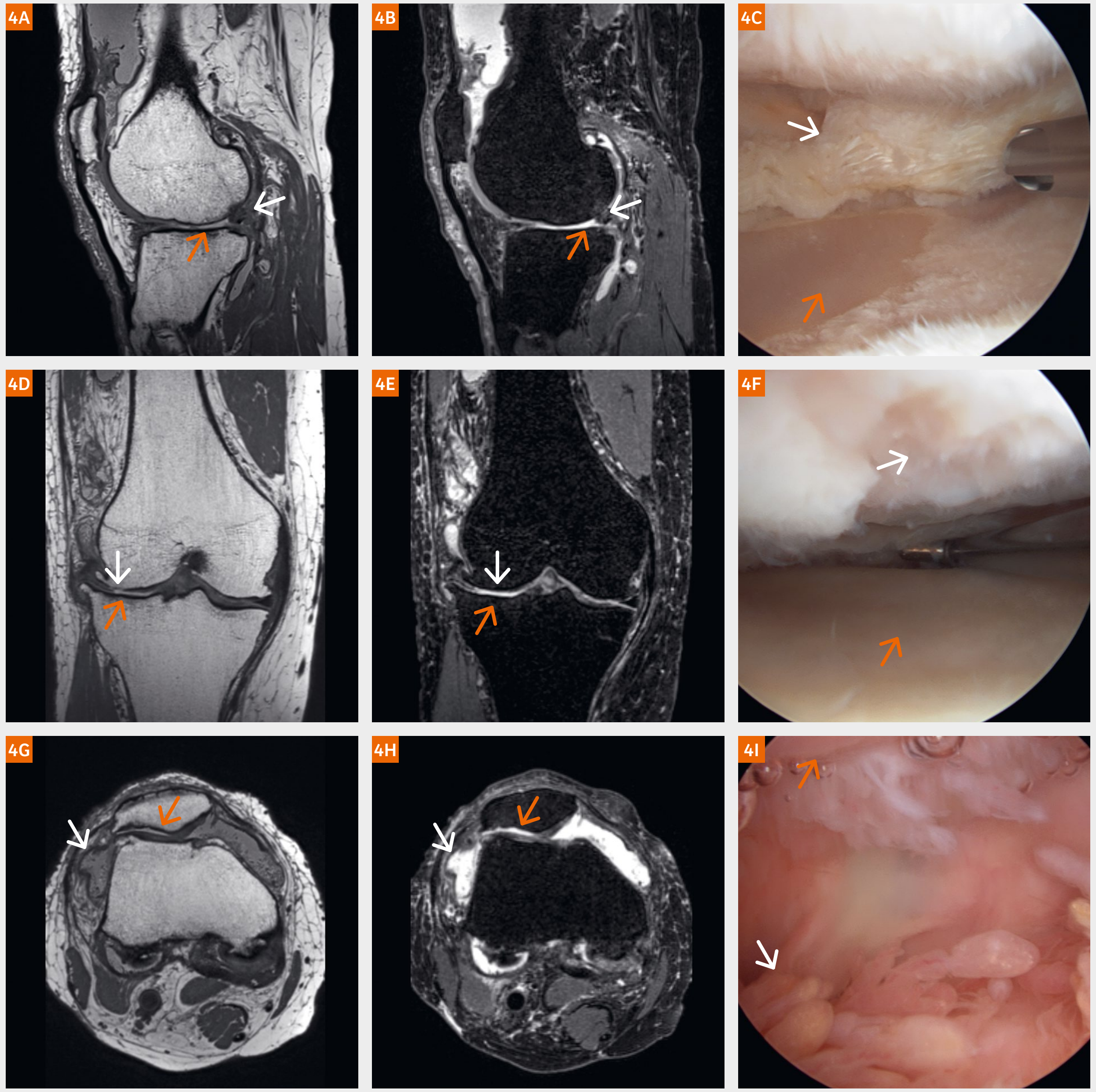

Indication: 60-year-old woman with intermittent pain and swelling of the right knee.

MRI findings: Sagittal, coronal, and axial intermediate-weighted and T2-SPAIR GOKnee3D images demonstrate a degenerative, complex tear of the posterior lateral meniscus (white arrows, **4A and 4B**). There is full-thickness cartilage loss over the lateral femoral condyle and lateral tibia plateau with focal bone-on-bone apposition (orange arrows, **4A and 4B**; white and orange arrows, **4D and 4E**). There is full-thickness cartilage loss of the lateral facet of the patella (orange arrow, **4G and 4H**) and synovitis with frond-like proliferations (white arrow, **4G and 4H**).

Arthroscopy findings: Degenerative, complex, tear of the posterior lateral meniscus (white arrow, **4C**). Full-thickness cartilage defects of the central femur (orange arrow, **4C and 4F**), tibia plateau (white arrow, **4F**), and lateral patella (orange arrow, **8I**) with synovitis (white arrow, **4I**).

Case 2

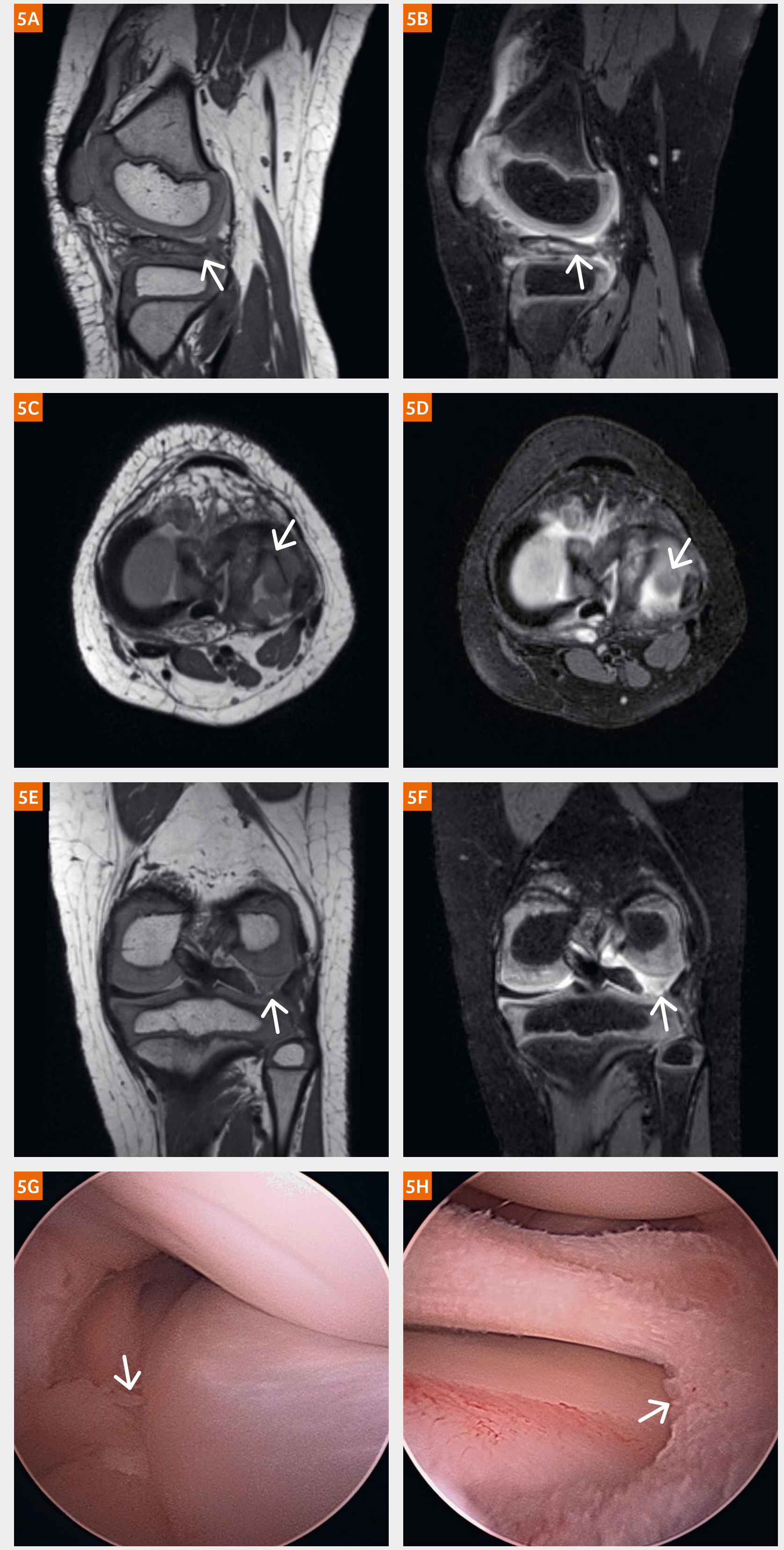

Indication: 4-year-old girl with mild knee pain and locking with motion.

MRI findings: Sagittal, coronal, and axial GOKnee3D images demonstrate a near complete discoid lateral meniscus with a complex tear (arrows). The medial meniscus, anterior and posterior cruciate ligaments, medial and lateral collateral ligaments, and articular cartilage are intact. There is a mild synovitis with small joint effusion.

Arthroscopy findings: Discoid lateral meniscus with a complex tear (arrow, **5G**), which was treated with resection of the tear and saucerization to create the crescent shape of a normal lateral meniscus **(5H)**.

Case 3

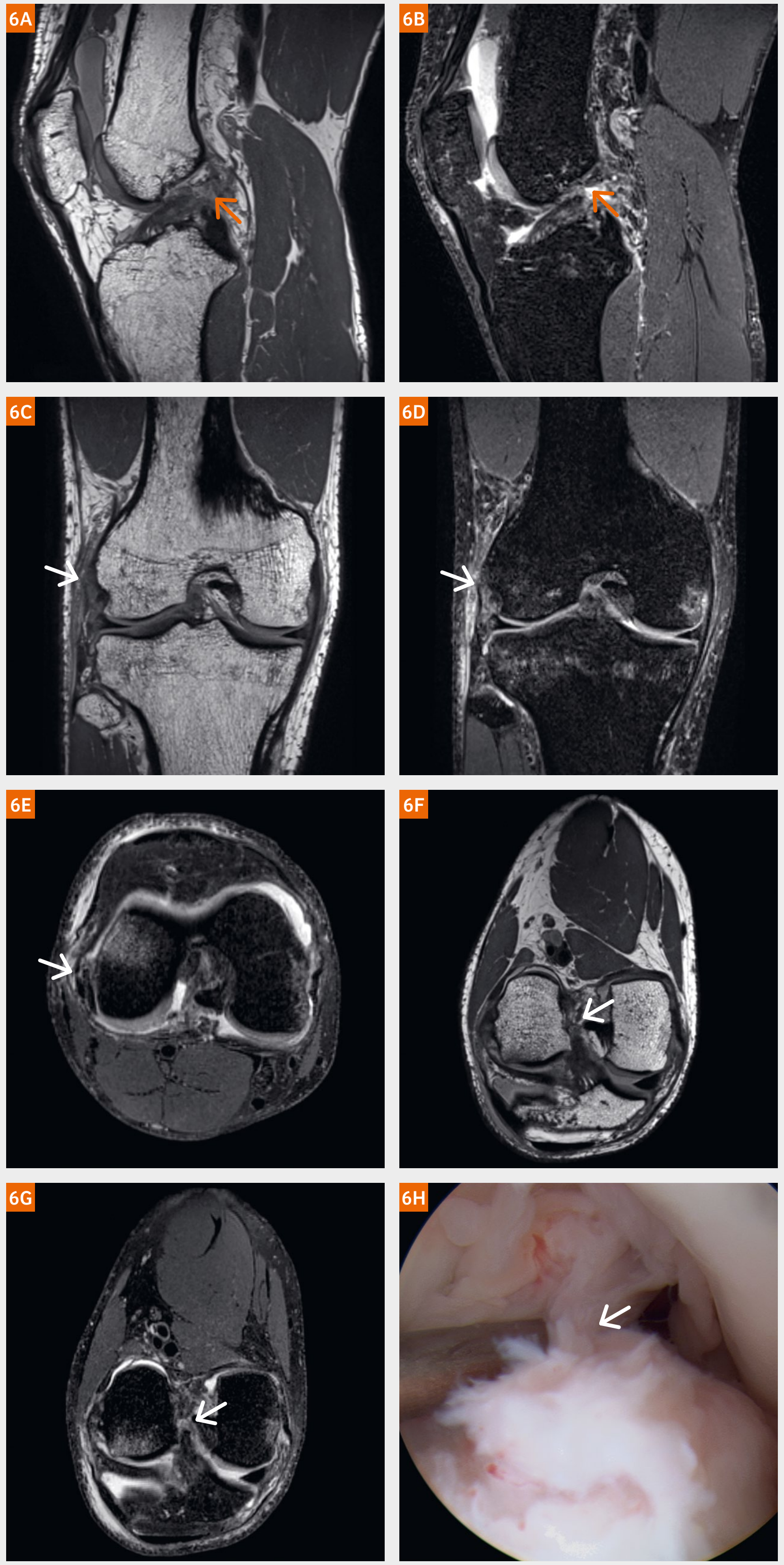

Indication: 30-year-old man with pain, swelling, and instability of the right knee following an American football injury.

MRI findings: Sagittal, coronal, axial and axial oblique GOKnee3D images demonstrate a full-thickness tear of the anterior cruciate ligament near the femoral attachment (arrow, **6A, B, F, G**). Additionally, there is a hemorrhagic joint effusion, a partial thickness tear of the lateral collateral origin (arrow, **6C–E**), and bone contusions of the femur and tibia.

Arthroscopy findings: Full-thickness tear of the anterior cruciate ligament near the femoral attachment (arrow, **6H**).

Case 4

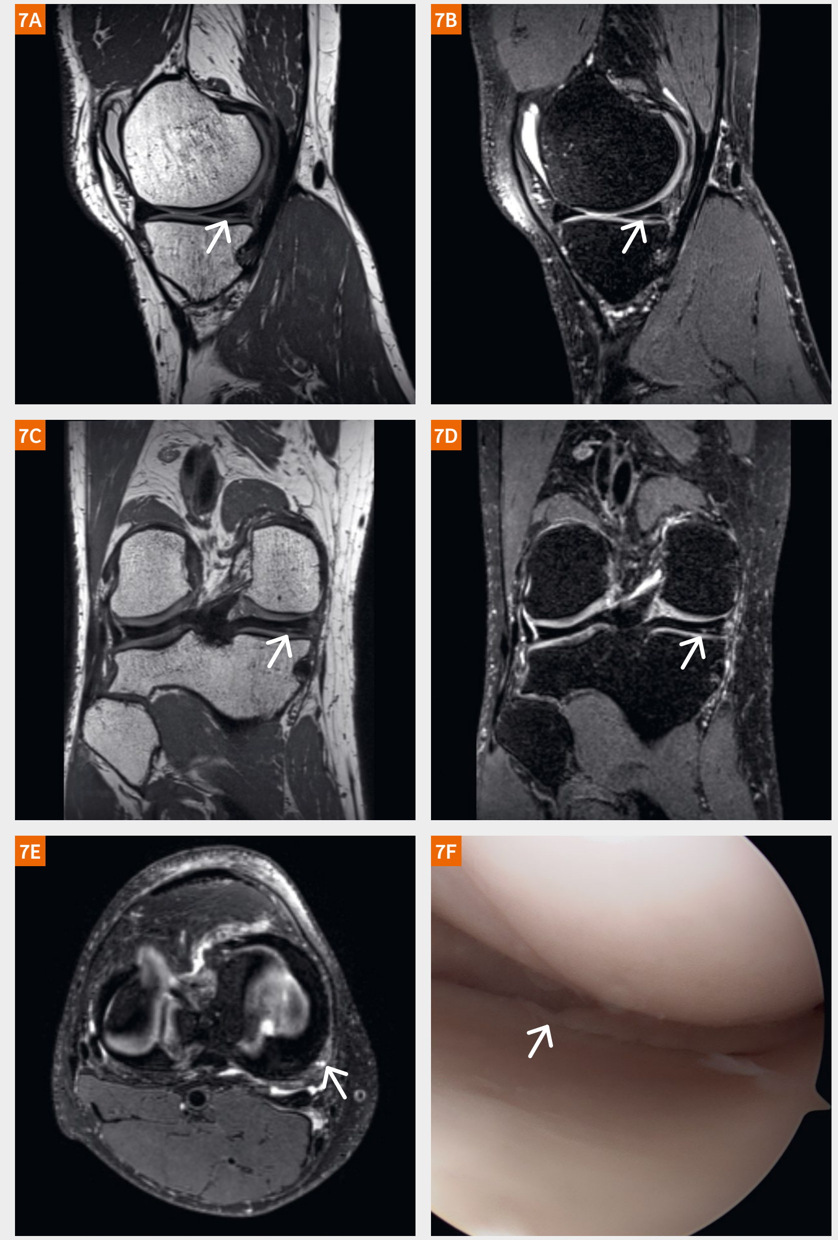

Indication: 52-year-old man with intermittent pain along the medial joint line of the knee.

MRI findings: Sagittal, coronal, and axial intermediate-weighted and T2-SPAIR GOKnee3D images demonstrate a complex, partial depth tear of the peripheral zone 1 of the posterior medial meniscus (arrows, **7A–D**). The meniscal tissue quality appears preserved. Additionally, there are small paramensical cysts at the location of the tear (arrow, **7E**).

Arthroscopy findings: Complex, partial depth tear of the peripheral zone 1 of the posterior medial meniscus (arrow, **7F**).

References

1 Horger W, Kiefer B. Fat suppression techniques – a short overview. MAGNETOM Flash 2011; 46: 56-59.
2 Breuer FA, Blaimer M, Mueller MF, Seiberlich N, Heidemann RM, Griswold M, Jakob PM. Controlled aliasing in volumetric parallel imaging (2D CAIPIRINHA). Mag Reson Med 2006; 55: 549-556.
3 Breuer F, Blaimer M, Griswold M, Jakob P. Controlled aliasing in Parallel Imaging Results IN Higher Acceleration (CAIPIRINHA). MAGNETOM Flash 2012; 49: 135-142.
4 Thawait GK, Lee RJ, Papp DF, Fritz J. High resolution isotropic 3D CAIPIRINHA SPACE MRI of the musculoskeletal system. MAGNETOM Flash 2016; 66: 30-38.
5 Fritz J, Fritz B, Thawait GG, Meyer H, Gilson WD, Raithel E. Three-Dimensional CAIPIRINHA SPACE TSE for 5-Minute High-Resolution MRI of the Knee. Invest Radiol. 2016 Oct;51(10):609-17.
6 Kalia V, Fritz B, Johnson R, Gilson WD, Raithel E, Fritz J. CAIPIRINHA accelerated SPACE enables 10-min isotropic 3D TSE MRI of the ankle for optimized visualization of curved and oblique ligaments and tendons. Eur Radiol. 2017 Sep;27(9):3652-3661.

Case 5

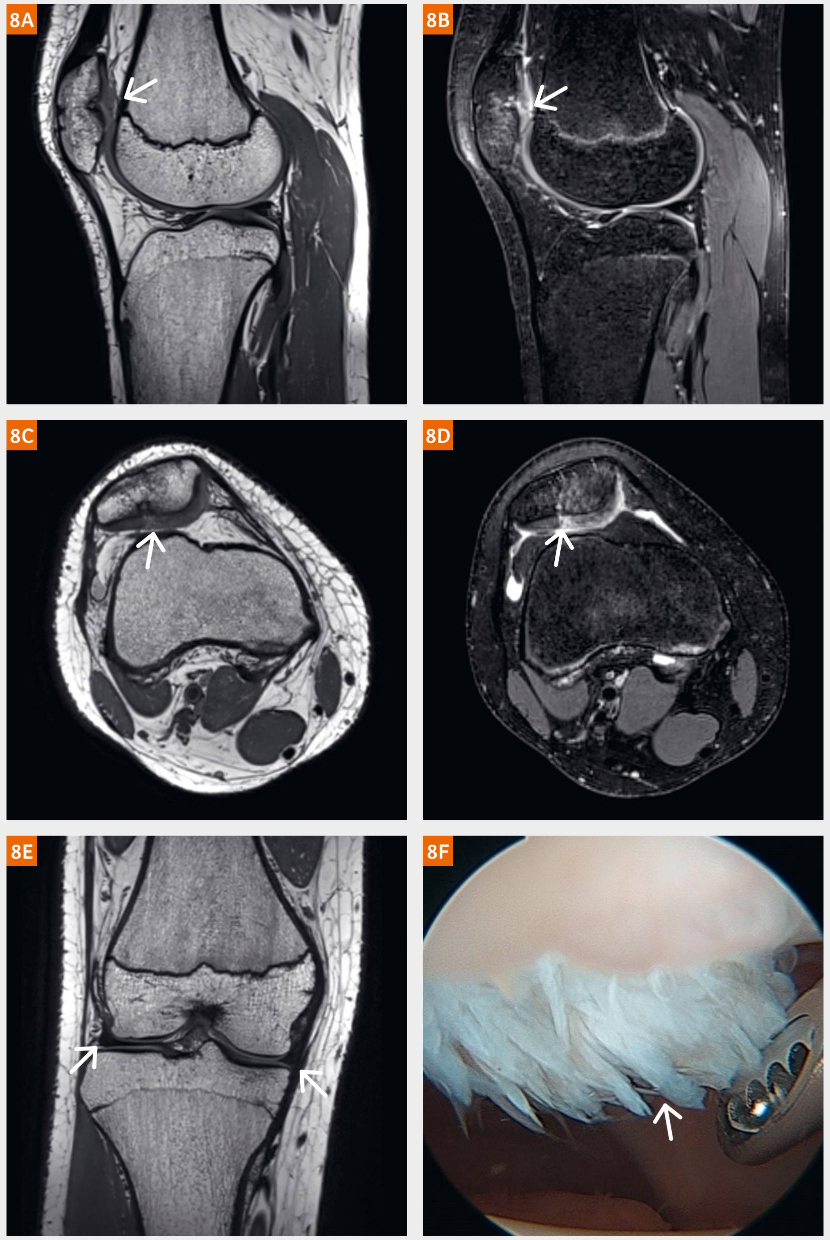

Indication: 14-year-old boy with anterior knee pain.

MRI findings: Sagittal, coronal, and axial oblique GOKnee3D images demonstrate patella alta alignment, hypoplasia of the trochlea, lateral patellar shift, and a full-thickness cartilage defect (arrows, **8A–D**) of the central patella with subcortical cyst formation and a small area of bone marrow edema pattern. There is a small joint effusion. The lateral and medial meniscus (arrows, **8E**) are intact.

Arthroscopy findings: Patellar chondromalacia with full-thickness cartilage defect (arrow, **8F**).

7 Rapalino O, Heberlein K. New strategies for protocol optimization for clinical MRI: Rapid examinations and improved patient care. MAGNETOM Flash 2016; 65: 22-25.
8 Prakkamakul S, Witzel T, Huang S, Boulter D, Borja MJ, Schaefer P, Rosen B, Heberlein K, Ratai E, Gonzalez G, Rapalino O. Ultrafast brain MRI: Clinical deployment and comparison to conventional brain MRI at 3T. J Neuroimaging 2016; 26(5): 503-510.
9 Fagundes J, Longo MG, Huang SY, Rosen BR, Witzel T, Heberlein K, Gonzalez RG, Schaefer P, Rapalino O. Diagnostic performance of a 10-minute gadolinium-enhanced brain MRI protocol compared with the standard clinical protocol for detection of intracranial enhancing lesions. Am J Neuradiol 2017; 38(9): 1689-1694.
10 Del Grande F and Fritz J. GOKnee3D Study. Unpublished data.
11 Fritz J, Ahlawat S, Thawait GK, Raithel E, Gilson W, Lee RJ. 3D MRI of Knee in Pediatric Patients with CAIPIRINHA SPACE: Diagnostic Performance Assessment with Arthroscopic Correlation. 25th ISMRM Annual Scientific Meeting & Exhibition; 2017; Hawaii, USA.

Case 6

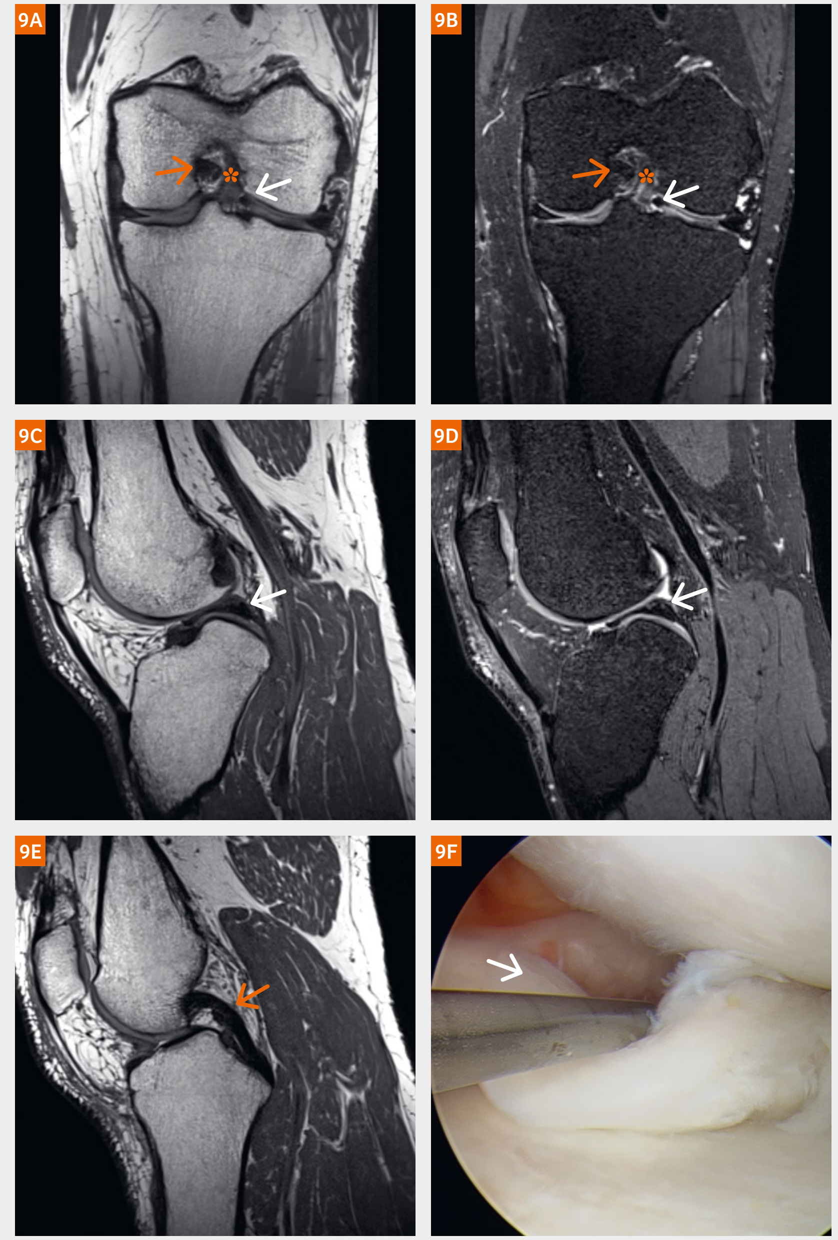

Indication: 51-year-old man with intermittent pain and locking of the left knee.

MRI findings: Sagittal and coronal intermediate-weighted and T2-SPAIR GOKnee3D images demonstrate a bucket handle tear of the lateral meniscus (white arrow, **9A–D**). The anterior cruciate ligament (asterisk, **9A–D**) and the posterior cruciate ligament (orange arrow, **9A** and **9B**) are intact.

Arthroscopy findings: Bucket handle tear of the lateral meniscus (arrow, **9F**).

Contact

Jan Fritz, M.D., P.D., D.A.B.R.
Director of Interventional MR Imaging
Associate Director MSK Fellowship
Assistant Professor of Radiology and Radiological Sciences
Johns Hopkins University School of Medicine
Russell H. Morgan Department of Radiology and Radiological Science
Musculoskeletal Radiology

601 N. Caroline Street, JHOC 3140A
Baltimore, MD 21287
USA
jfritz9@jhmi.edu

Learn from the experience of other MAGNETOM users

The MAGNETOM World is the community of Siemens Healthineers MR users worldwide, providing you with relevant clinical information. Here you will find application tips and protocols to optimize your daily work.

Lectures and presentations from experts in the field will allow you to be exposed to new ideas and alternative clinical approaches.

Put the advantages of the MAGNETOM World to work for you!

www.siemens.com/magnetom-world

Optimize your clinical protocols by downloading the .exar1 and .edx files shared by leading institutions around the world.

Go to **Clinical Corner > Protocols**

Musculoskeletal MRI

Download musculoskeletal MRI protocols.

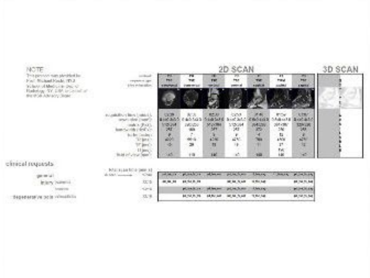

MSK Advisory Board

Find here MR imaging parameters, protocols and application tips including videos.

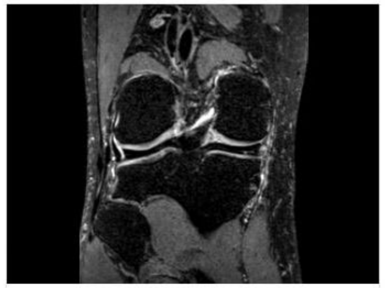

GOKnee3D Protocols

Fast high-res 3D knee exams in 10 min. Download .exar1 files for MAGNETOM Aera and Skyra.

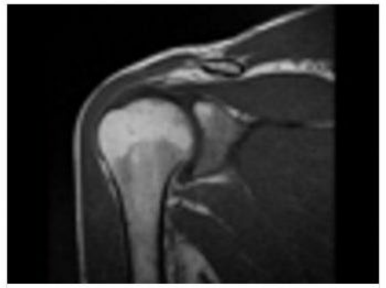

Shoulder Protocols with Flex 4 Coil

Download .exar1 file of the shoulder with Flex 4 coil for 1.5T MAGNETOM Amira and Sempra.

T1w

Dowr protc

Don't miss the talks of international experts on all aspects of MRI in MSK.

Go to **Clinical Corner > Clinical Talks**

MRI of joint replacements

Reto Sutter, M.D., Balgrist University Hospital, Zurich, Switzerland, 10[th] *MAGNETOM World Summit*

MRI for the detection and grading of muscle injuries

Marc-André Weber, M.D., University Medicine Rostock, Germany, 10[th] *MAGNETOM World Summit*

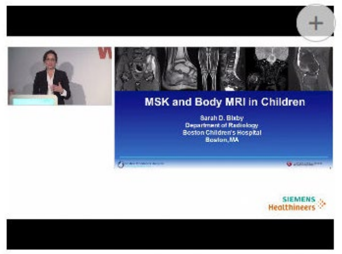

MSK and Body MRI in Children

Sarah D. Bixby, M.D., Boston Children's Hospital, Boston, MA, USA, 10[th] *MAGNETOM World Summit*

The centerpiece of the MAGNETOM World Internet platform consists of MAGNETOM users' clinical results. Here you will find articles, case reports and clinical methods.

Go to **Clinical Corner > Case Studies**

Nov 25, 2016

Christopher J. Hanrahan et al.
Department of Radiology and Imaging Sciences, University of Utah School of Medicine, Salt Lake City, UT, USA

Utility of MRI Findings in Inflammatory Myopathies

Nov 25, 2016

Gustav Andreisek, M.D., MBA et al.
Radiology, Spital Thurgau, Münsterlingen, Switzerland, University of Zurich, Switzerland

Review: MRI of Muscle Denervation Syndromes

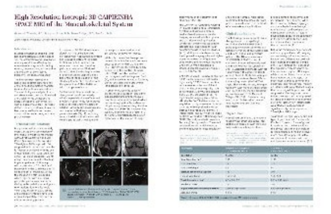

Nov 25, 2016

Jan Fritz, M.D., P.D., D.A.B.R. et al.
Johns Hopkins University School of Medicine, Baltimore, MD, USA

High Resolution Isotropic 3D CAIPIRINHA SPACE MRI of the Musculoskeletal System

Just a mouse click away you will find application videos and useful tips allowing you to optimize your daily MR examinations.

Go to **Clinical Corner > Application Tips**

Apr 30, 2014

Wilhelm Ruempler, M.D.
Klinik Dr. Hancken, Stade, Germany

Improving MR Joint Diagnostics with T1 Water Contrast Using a RESTORE Pulse

Apr 22, 2013

Elena Ferrer; et al.
Radiology Department, Clinica Creu Blanca, Barcelona, Spain,

MSK Imaging at 3T with Simultaneous Use of Multipurpose Loop Coils

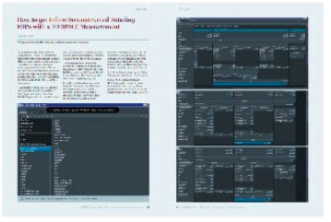

Nov 29, 2015

Thomas Illigen
Siemens Healthcare GmbH, Mannheim, Germany

How to get Inline Reconstructed Rotating MIPs with a 3D SPACE Measurement

Metal Artifact Reduction Sequence (MARS) Magnetic Resonance Neurography (MRN) Evaluation of the Lumbosacral Plexus in Patients with Metallic Implants

Shivani Ahlawat, M.D.; Jan Fritz, M.D., P.D., D.A.B.R.

Johns Hopkins University School of Medicine, Baltimore, MD, USA

Abstract

Magnetic resonance neurography (MRN) is a reliable and accurate modality in the assessment of patients with peripheral neuropathy, which can be useful for distinguishing intrinsic and extrinsic etiologies of neuropathy following surgery. However, MRN surrounding metal implants[1] can be challenging to both perform and interpret. The diagnosis of abnormal peripheral nerves often heavily relies on fluid sensitive MR pulse sequences, but the presence of metal in the field of view introduces image artifacts, distortion and interferes with fat suppression. Conventional turbo spin echo pulse sequences with optimization for metal artifact reduction[1] are best suited for nerve imaging as advanced multi-spectral, and multi-spatial pulse sequences introduce a degree of blur that obscure nerve details. As such, metal artifact reduction sequence (MARS) techniques[1] can be applied to improve the image quality of MRN in patients with pelvic metallic implants, when compared with standard fast spin echo sequences. We describe a high-resolution MARS MRN protocol that yields high image quality and validated diagnostic accuracy for the assessment of lumbosacral neuropathies in patients with metallic implants of the pelvis and hips.

	Intermediate-weighted Turbo Spin Echo	STIR Turbo Spin Echo
Orientation	transversal	transversal
Repetition time [ms]	5700	3660
Time to echo [ms]	38	6.9
Inversion time [ms]	-	150
Echo train length	16	16
Slice thickness/gap [mm]	4.5/0.45	5/0.5
Pixel size [mm^2]	0.5 x 0.5	0.7 x 0.7
Bandwidth [Hz/px]	560	545
Flip angle [degree]	150	130
Number of slices	2 x 35	2 x 27
Number of excitations	1.5	2
In-plane frequency encoding direction	Right to left	Right to left
Total acquisition time [min:sec]	8:42	13:36

Table 1:
Detailed MARS MR imaging protocol optimized for the evaluation of lumbosacral plexus and pelvic nerves in patients with metallic implants[1].

Introduction

Traumatic nerve palsy in the setting of previous pelvic instrumentation and hip arthroplasty is a rare but serious complication [1–9]. Diverse mechanisms of peripheral nerve injury have been described including lesions intrinsic and extrinsic to the affected peripheral nerve. Intrinsic causes of peripheral neuropathy in the postoperative setting include stretch injury, nerve lacerations, and vascular compromise. Extrinsic causes of peripheral neuropathy in the postoperative setting include mass effect by implant components, heterotopic ossification, fluid collections such as hematoma, distended peri-articular bursae, and abscesses, and adverse local tissue reactions. The current standard of care for the detection and characterization of peripheral neuropathy is clinical examination and electrodiagnostic testing. However, evaluation of sensory and deep intra-pelvic nerves can be challenging, representing a gap in the clinical management of patients with a pelvic peripheral nerve injury in the post-operative setting.

[1] The MRI restrictions (if any) of the metal implant must be considered prior to patient undergoing MRI exam. MR imaging of patients with metallic implants brings specific risks. However, certain implants are approved by the governing regulatory bodies to be MR conditionally safe. For such implants, the previously mentioned warning may not be applicable. Please contact the implant manufacturer for the specific conditional information. The conditions for MR safety are the responsibility of the implant manufacturer, not of Siemens.

Magnetic resonance neurography (MRN) is a reliable and accurate modality for the assessment of patients with peripheral neuropathy that can be useful for identifying intrinsic or extrinsic etiologies of neuropathy. However, the presence of metal in the field-of-view generates local magnetic field heterogeneity and results in image artifacts including signal voids, failure of fat suppression, and spatial misregistration [10]. As such, MR imaging surrounding metal implants, including arthroplasty and osteosynthesis implants, can be challenging to interpret [10]. Metal artifact reduction strategies include the use of lower magnetic field strength, such as 1.5 instead of 3 Tesla, turbo spin echo (TSE) rather than gradient echo based sequences, high receiver bandwidth, and inversion recovery rather than frequency-selective fat suppression [10–19]. The application of such metal artifact reduction sequence (MARS) techniques results in substantially improved image quality when compared with standard TSE pulse sequences [12].

TSE pulse sequences with optimization for metal artifact reduction are ideal for peripheral nerve imaging as advanced multi-spectral and multi-spatial pulse sequences, such as Multi-acquisition Variable-resonance Image Combination (MAVRIC, GE Healthcare, Wauwatosa, WI, USA) and Slice Encoding for Metal Artifact Correction (SEMAC) introduce a degree of blurring that can obscure the fine architecture of peripheral nerves [12, 1]. We describe a validated, high-resolution MARS MRN protocol that yields high image quality and accuracy for the diagnosis of lumbosacral neuropathies in patients with metallic implants of the pelvis and hips [20].

MARS MRN acquisition

At our institution, we perform MARS MRN of the lumbosacral plexus for the evaluation of patients with metallic implants on a 1.5 Tesla MR imaging system (MAGNETOM Aera, Siemens Healthcare, Erlangen, Germany) with 48 radio-frequency receive channels, 45 mT/m maximum gradient field amplitude and 200 T/m/s slew rate [20]. Patients are positioned supine, and imaging is acquired using two 18-channel receive-only body matrix surface coils (Siemens Healthcare) and 12 elements of a spine matrix coil in 'sandwich configuration' to cover the lower lumbar spine, pelvis and proximal thighs. Table 1 describes the imaging protocol in detail (Fig. 1). The short tau inversion recovery (STIR)

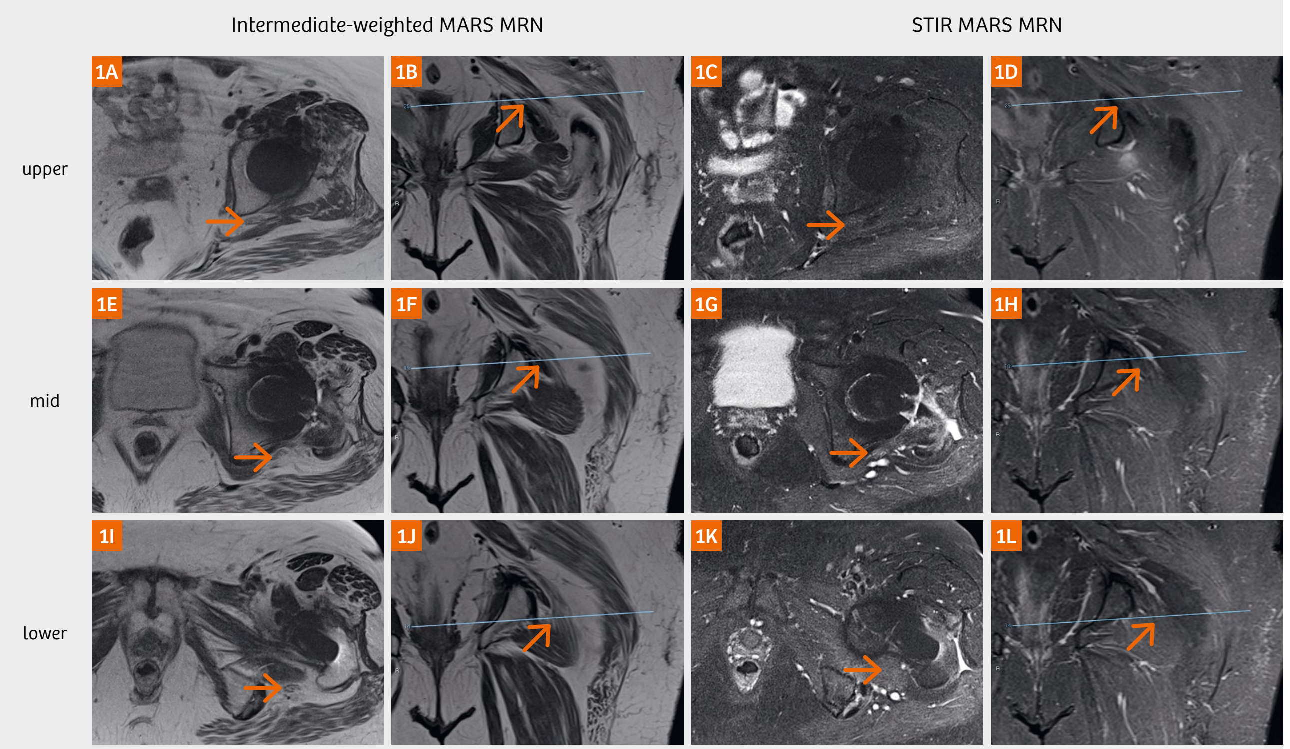

Figure 1:
Metal Artifact Reduction Magnetic Resonance Neurography in a patient with left hip arthroplasty implants demonstrates a normal appearing sciatic nerve (arrows) at the upper, mid and lower levels (reference lines) of the hip replacement without obscuration by implant-induced artifacts and with solid fat suppression.

TSE pulse sequence employs a radio-frequency pulse that matches the high receiver bandwidth [16]. Because the field-of-view extends from the L5 vertebral body to the ischial tuberosity, contiguous stacks of axial intermediate-weighted and STIR TSE pulse sequences are obtained. Intravenous contrast material administration is typically not required. The total acquisition time of the axial pulse sequences of this particular MARS MRN protocol is approximately 25 minutes, predominantly due to the long acquisition time necessary for high-quality STIR images. Optional coronal or sagittal pulse sequences can be helpful to identify landmarks for surgical interventions. The length of this protocol may be difficult to tolerate for acutely ill patients, but is similar to other investigations [14, 15, 20].

MARS MRN Interpretation

There is a paucity of literature of MRN in the setting of metal implants [19–21]. Our validated MARS MRN protocol offers high diagnostic quality, inter-rater agreement and overall high diagnostic accuracy for the presence of MR features of neuropathy [20]. With this MARS MRN protocol, both primary and secondary features of peripheral neuropathy can be visualized at the level of many metallic implants.

Primary features of peripheral neuropathy include abnormal course, caliber, signal intensity, and architecture (Fig. 2). Secondary features of peripheral neuropathy include skeletal muscle denervation. Of note, elevated

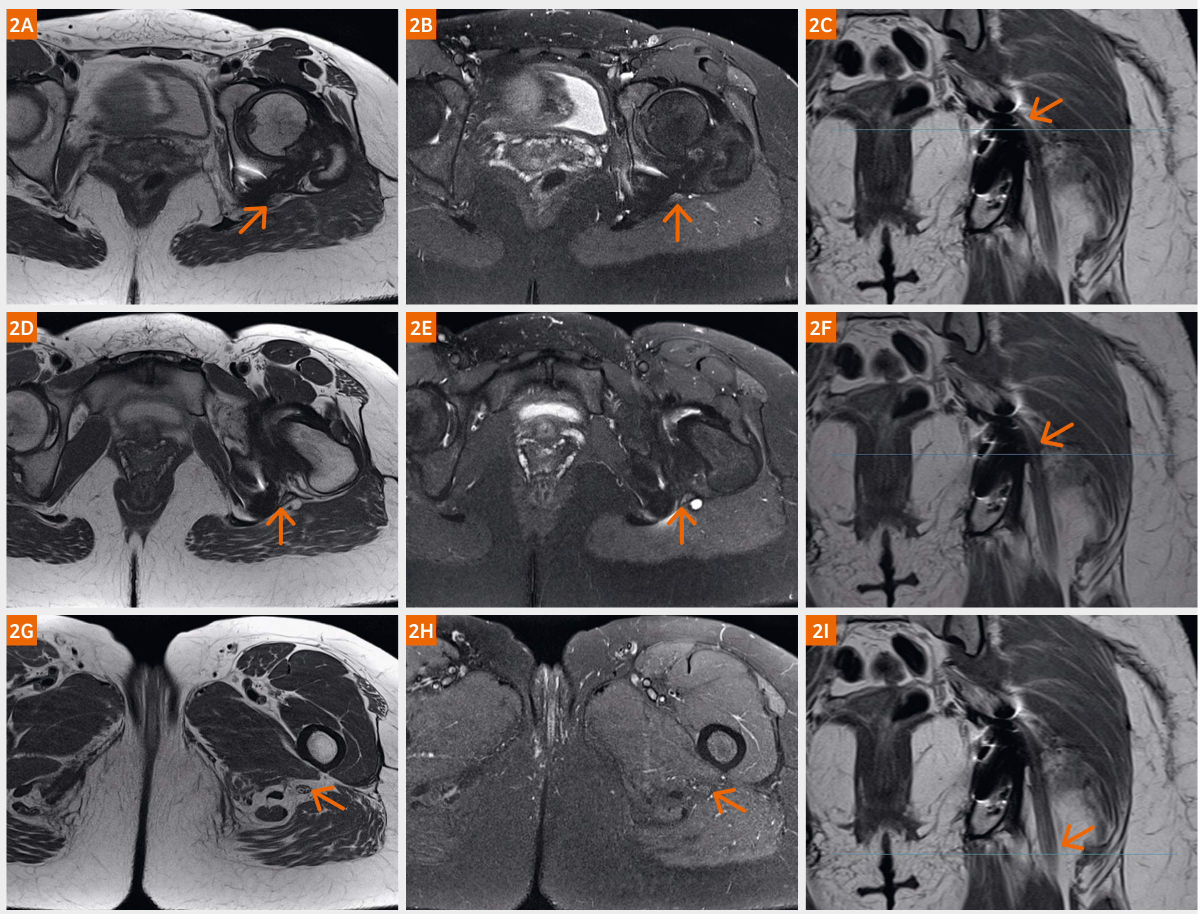

Figure 2:
Metal Artifact Reduction Magnetic Resonance Neurography in a patient with prior pelvic osteosynthesis and metallic implants of the left posterior acetabulum and ischium demonstrates unilateral, abnormal signal hyperintensity of the left sciatic nerve (arrow, **2A–C**), indicating neuropathy. At the mid level, there is unilateral left perineural scarring and tethering of the sciatic nerve (arrows, **2D–F**) to the metallic implants, as well as abnormal signal hyperintensity of the nerve. At the lower level, below of the site of surgical instrumentation, the sciatic nerve (arrow, **2G–I**) is normal in morphology and signal intensity.

peripheral nerve signal on fluid sensitive sequences alone is common, but not necessarily a reliable finding, that can result in high sensitivity but low specificity, when used in isolation, [22, 23]. The presence of additional imaging features such as abnormal nerve caliber including flattening and enlargement can add specificity [23]. Bulbous enlargement and architectural distortion in otherwise longitudinally intact nerves may suggest the presence of a traumatic neuroma-in-continuity [9]. Lastly, nerve discontinuity can serve as a marker for a high-grade peripheral nerve injury or nerve laceration, which are rare causes of neuropathy in the postoperative setting [9].

Concerning secondary features of peripheral neuropathy, MARS MRN can detect and characterize the extent of skeletal muscle denervation, if the muscles of interest are included, which may require adding additional stacks of images. MRN features of skeletal muscle denervation include intramuscular edema-like signal, fatty replacement, and loss of muscle bulk. Skeletal muscle atrophy and fatty replacement have been described in patients following hip arthroplasty and can be present in asymptomatic patients [21]. Hence, it is important to interpret MARS MRN in the individual clinical context rather than in isolation.

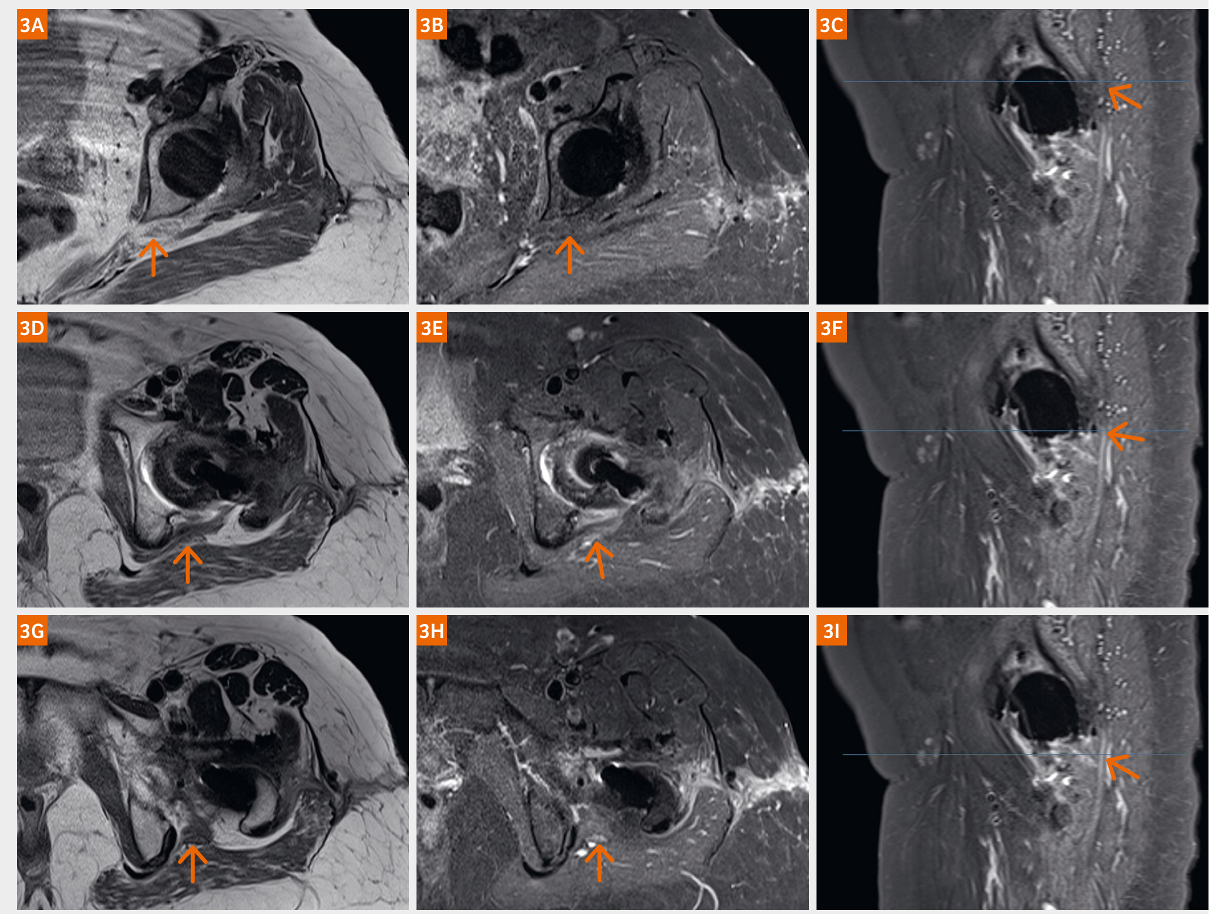

Figure 3:
Metal Artifact Reduction Magnetic Resonance Neurography in a patient with new-onset foot extension and flexion weakness following recent left hip arthroplasty demonstrates normal morphology and signal hyperintensity of the left sciatic nerve (arrow, **3A–C**) at the upper level. At the mid level, there is abnormal signal hyperintensity of the sciatic nerve (arrows, **3D–F**) in the subgluteal space. At the lower level, there is perineural scarring of the sciatic nerve and abnormal signal intensity of the sciatic nerve (arrow, **3G–I**), indicative of neuropathy.

Reprinted from MAGNETOM Flash (69) 3/2017
www.siemens.com/magnetom-world

Lastly, MARS MRN also demonstrates the soft tissues surrounding the pelvic nerves, including perineural fibrosis (Fig. 3), collections causing course deviations and mass effect, which can provide added value to electrodiagnostic testing and the clinical management of these patients.

Conclusion

MARS MRN provides high image quality of the pelvic peripheral nerves and lumbosacral plexus with validated accuracy for the diagnosis of lumbosacral plexopathy in patients with metallic pelvic implants.

References

1 Burge AJ, Gold SL, Kuong S, Potter HG. High-resolution magnetic resonance imaging of the lower extremity nerves. Neuroimaging Clin N Am. 2014;24(1):151-70.
2 Brown GD, Swanson EA, Nercessian OA. Neurologic injuries after total hip arthroplasty. Am J Orthop 2008;374:191-197.
3 Farrell CM, Springer BD, Haidukewych Gj, Morrey BF Motor nerve palsy following primary total hip arthroplasty. J Bone Joint Surg Am 2005; 87(12):2619-2625.
4 Navarro RA, Schmalzried TO, Amstutz HC, Dorey FJ Surgical approach and nerve palsy in total hip arthroplasty. J Arthroplasty 1995; 10:1-5.
5 Zappe B, Glauser PM, Majewski M, Stöckli HR, Ochsner PE. Long-term prognosis of nerve palsy after total hip arthroplasty: results of two-year-follow-ups and long-term results after a mean time of 8 years. Arch Orthop Trauma Surg. 2014;134:1477-82.
6 Schmalzried TP, Amstutz HC, Dorey FJ. Nerve palsy associated with total hip replacement. Risk factors and prognosis. J Bone Joint Surg Am. 1991;73:1074-80.
7 Melamed NB, Satya-Murti. S. Obturator neuropathy after total hip replacement. Ann Neurol. 1983;13:578-9.
8 Weber ER, Daube JR, Coventry MF. Peripheral neuropathies associated with total hip arthroplasty. J Bone Joint Surg [Am] 1976;58:66-69.
9 BN Edwards, Tullos HS, Noble PC. Contributory factors and etiology of sciatic nerve palsy in total hip arthroplasty. Clin Orthop 1987; 218:136.
10 Fritz J, Lurie B, Miller TT, Potter HG. MR Imaging of Hip Arthroplasty Implants. Radiographics. 2014; 34(4): E106-132.
11 Potter HG, Nestor BJ, Sofka CM, Ho ST, Peters LE, Salvati EA. Magnetic resonance imaging after total hip arthroplasty: evaluation of periprosthetic soft tissue. J Bone Joint Surg Am; 2004(86):1947–1954.
12 Hayter CL, Koff MF, Shah P, Koch KM, Miller TT, Potter HG. MRI after arthroplasty: comparison of MAVRIC and conventional fast spin-echo techniques. AJR Am J Roentgenol 2011;197: W405–W411.
13 Hayter CL, Koff MF, Potter HG. Magnetic resonance imaging of the postoperative hip. J Magn Reson Imaging 2012;35:1013–1025
14 Fritz J, Ahlawat S, Demehri S, Thawait GK, Raithel E, Gilson WD, Nittka M.Compressed Sensing SEMAC: 8-fold Accelerated High Resolution Metal Artifact Reduction MRI of Cobalt-Chromium Knee Arthroplasty Implants. Invest Radiol. 2016;51(10):666-76.
15 Fritz J, Fritz B, Thawait GK, Raithel E, Gilson WD, Nittka M, Mont MA. Advanced metal artifact reduction MRI of metal-on-metal hip resurfacing arthroplasty implants: compressed sensing acceleration enables the time-neutral use of SEMAC. Skeletal Radiol. 2016 Oct;45(10):1345-56.
16 Ulbrich EJ, Sutter R, Aguiar RF, Nittka M, Pfirrmann CW. STIR sequence with increased receiver bandwidth of the inversion pulse for reduction of metallic artifacts. AJR Am J Roentgenol. 2012 Dec;199(6):W735-42.
17 Sutter R, Ulbrich EJ, Jellus V, Nittka M, Pfirrmann CW. Reduction of metal artifacts in patients with total hip arthroplasty with slice-encoding metal artifact correction and view-angle tilting MR imaging. Radiology 2012;265:204–214.
18 Muller GM, Lundin B, von Schewelov T, Muller MF, Ekberg O, Mansson S. Evaluation of metal artifacts in clinical MR images of patients with total hip arthroplasty using different metal artifact reducing sequences. Skeletal Radiol. 2015:44:353-09.
19 Wolf M, Bäumer P, Pedro M, Dombert T, Staub F, et al. Sciatic Nerve Injury Related to Hip Replacement Surgery: Imaging Detection by MR Neurography Despite Susceptibility Artifacts. PLoS ONE 2014;92: e89154.
20 Ahlawat S, Stern SE, Belzberg AJ, Fritz J. High-resolution metal artifact reduction MR imaging of the lumbosacral plexus in patients with metallic implants. Skeletal Radiol. 2017 Jul;46(7):897-908.
21 Pfirrmann CW, Notzli HP, Dora C, Hodler J, Zanetti M. Abductor tendons and muscles assessed at MR imaging after total hip arthroplasty in asymptomatic and symptomatic patients. Radiology 2005;235:969–976.
22 Chhabra A, Chalian M, Soldatos T, Andreisek G, Faridian-Aragh N, Williams E, Belzberg AJ, Carrino JA. 3-T high-resolution MR neurography of sciatic neuropathy. AJR Am J Roentgenol. 2012;1984:W357-64.
23 Kwee RM, Chhabra A, Wang KC, Marker DR, Carrino JA. Accuracy of MRI in diagnosing peripheral nerve disease: a systematic review of the literature. AJR Am J Roentgenol. 2014;203:1303-9.
24 Ahlawat S, Belzberg AJ, Montgomery EA, Fayad LM. MRI features of peripheral traumatic neuromas. Eur Radiol. 2016;26:1204-12.

Contact

Shivani Ahlawat, M.D.
Director MSK Fellowship
Assistant Professor of Radiology and Radiological Sciences
Johns Hopkins University School of Medicine
Russell H. Morgan Department of Radiology and Radiological Science
Musculoskeletal Radiology
601 N. Caroline Street
Baltimore, MD 21287, USA
sahlawa1@jhmi.edu

Jan Fritz, M.D., P.D., D.A.B.R.
Director of Interventional MR Imaging
Associate Director MSK Fellowship
Assistant Professor of Radiology and Radiological Sciences
Johns Hopkins University School of Medicine
Russell H. Morgan Department of Radiology and Radiological Science
Musculoskeletal Radiology
601 N. Caroline Street, JHOC 3140A
Baltimore, MD 21287, USA
jfritz9@jhmi.edu